Annu. Rev. Fluid Mech. 1999. 31:55–93

TRANSPORT BY COHERENT BAROTROPIC VORTICES

Antonello Provenzale
Istituto di Cosmogeofisica del CNR, Corso Fiume 4, I-10133 Torino, Italy;
e-mail: anto@icg.to.infn.it

KEY WORDS: coherent structures, turbulence, transport, geophysical fluid dynamics, chaotic advection

ABSTRACT

This article reviews the transport properties of coherent vortices in rotating barotropic flows. It is shown that vortices induce regular Lagrangian motion inside their cores and are highly impermeable to inward and outward particle fluxes. Passive tracers can be trapped inside vortex cores for long times and are transported by the vortex motion over large distances. Absolute dispersion in vortex-dominated flows is discussed by studying particle dynamics in 2D turbulence, point-vortex systems, and subsurface float trajectories in the ocean. Finally, it is shown that anticyclonic coherent vortices in cyclonically rotating reference frames can concentrate heavy impurities (e.g. dust grains) in their cores. This process may play an important role in the formation of planetesimals in the early solar nebula.

1. *Introduction*

Whenever rotating turbulent flows have been observed with sufficient resolution, long-lived coherent vortices have been detected (Bengston & Lighthill 1982, Dowling & Spiegel 1990, Ingersoll 1990, Hopfinger & van Heijst 1993, Nezlin & Snezhkin 1993, McWilliams & Weiss 1994). Examples include Gulf Stream rings and salty Mediterranean eddies in the ocean (MODE Group 1978, Ring Group 1981, Wunsch 1981, Malanotte Rizzoli 1982, McWilliams 1985, Flierl 1987, Armi et al 1989, Richardson et al 1989, 1991), the polar vortex (e.g. McIntyre 1989, 1995) and tropical cyclones (Rossby 1949, Adem 1956, Chan & Williams 1987), rotating plumes in turbulent convection (Killworth 1983, Brummell et al 1996, Julien et al 1996), great spots on giant planets such

0066-4189/99/0115-0055$08.00

as the Great Red Spot on Jupiter (e.g. Ingersoll 1990, Dowling 1995), dark and bright star spots where rotation and magnetic fields both play a role (Dowling & Spiegel 1990), and perhaps vortex spots on astrophysical disks (Abramowicz et al 1991, Bracco et al 1998).

Coherent vortices form naturally in rotating flows, as many numerical simulations and laboratory experiments have shown. A random initial vorticity field can organize itself into long-lived vortices that dominate the dynamics of the flow and emerge as individual coherent entities from the turbulent background (McWilliams 1984). The formation of coherent vortices is usually associated with the presence of an inverse cascade of a crucial dynamical quantity (typically, energy) from small to large scales. However, the inverse cascade in itself is not enough to explain why coherent vortices are generated. Although various possible motivations have been suggested (e.g. Leith 1984, Robert & Sommeria 1991, Chavanis & Sommeria 1996) a fully satisfactory theory of vortex formation is still missing.

Nevertheless, vortices are there, and influence the dynamics in many ways. In particular, coherent vortices are very efficient in trapping passive tracers for long times and transporting them over large distances (Elhmaidi et al 1993). Coherent vortices can thus play an important role in global transport processes in rotation-dominated flows, such as large-scale geophysical flows.

At present, general circulation models of the ocean and the atmosphere do not resolve the full spectrum of "eddies" that are present in the system, and rely upon some form of parameterization of the eddy activity (e.g. Danabasoglu et al 1994, McWilliams 1996). For coherent vortices, simple parameterizations based on eddy diffusion concepts do not necessarily provide the correct answer. As a consequence, it is necessary first to understand transport by coherent vortices and then to properly parameterize it. In the last few years, the dynamics and transport properties of coherent vortices have been studied in some detail, particularly in the case of barotropic flows. This has lead to a fairly complete understanding of the transport associated with barotropic coherent vortices, which is reviewed here. As often claimed in short reviews like this one, no completeness is guaranteed, and these notes barely represent my personal view of the subject.

2. *Dynamics of Barotropic Turbulence*

In the following, I consider the simplest nontrivial system exhibiting complex spacetime evolution and the presence of coherent vortices, namely, barotropic turbulence in the quasigeostrophic (QG) approximation (e.g. Charney 1971, Rhines 1979, Pedlosky 1987). In the rest of this paper, this system will be our prototype for the study of transport by coherent vortices.

In quasigeostrophic turbulence, the fluid motion is supposed to be rotation-dominated and two-dimensional in a shallow layer, on a local horizontal plane.

The rotation axis of the reference frame is perpendicular to the plane of motion. The flow is divergenceless and the horizontal velocity is expressed in terms of a stream function. All vertical derivatives and the vertical velocity vanish. In the barotropic approximation, the density of the fluid is homogeneous and no baroclinicity is present.

For quasigeostrophic motions in the ocean and the atmosphere, a local Cartesian approximation is often used. The relevant rotation parameter becomes the Coriolis parameter $f = 2\Omega \sin\theta$, where Ω is the rotation frequency of the Earth, and θ is latitude. Local Cartesian variables are $x = (\phi - \phi_0) R_E \cos\theta_0$ in the zonal (East-West) direction, $y = (\theta - \theta_0) R_E$ in the meridional (North-South) direction, and z in the local vertical direction. Here, ϕ is longitude, ϕ_0 and θ_0 are respectively a reference longitude and latitude at the center of the domain of interest, and R_E is the radius of the Earth. In the QG approximation, only the local vertical projection of the Earth's rotation vector is taken into account; this approximation looses validity near the equator.

On a spherical planet, the local vertical projection of the rotation vector varies with latitude. Differential rotation is thus present when employing a local Cartesian approximation. If the fluid motion takes place on scales smaller than those where the effects of differential rotation have influence, the variation of the Coriolis parameter with latitude (i.e. with y) may be discarded, using what is called the f-plane approximation. In this case, the Coriolis parameter simply becomes $f \equiv f_0 = 2\Omega \sin\theta_0$. If the latitude dependence of f cannot be discarded, a possible approach is provided by the β-plane approximation, which is based on considering the locally linearized variation of the Coriolis parameter with latitude. That is, $f \equiv f_0 + \beta y$, where $\beta = 2\Omega \cos\theta_0 / R_E$.

The equation of motion for a rotation-dominated homogeneous fluid layer on a flat bottom topography and with a free surface is written in dimensionless variables as

$$\frac{Dq}{Dt} = \frac{\partial q}{\partial t} + [\psi, q] = F + D, \tag{1}$$

where

$$q = \omega + f_0 + \beta y - \psi / R^2 \tag{2}$$

is potential vorticity, and $D/Dt = \partial/\partial t + [\psi,]$ is the total advective derivative. Here, $\omega = \nabla^2 \psi$ is relative vorticity, ψ is the stream function which is proportional to the elevation of the free surface, $[\psi, q] = \partial_x \psi \partial_y q - \partial_x q \partial_y \psi$ is the Jacobian operator, and F and D are forcing and dissipation terms respectively.

The parameter R is the dimensionless Rossby deformation radius expressed in units of the domain size, $R = R_0/L$, where $R_0 = (gH)^{1/2}/f_0$ is the dimensional Rossby deformation radius. Here g is the acceleration of gravity (in the z

direction), H is the average depth of the fluid layer, and L is the horizontal size of the domain. The flow described by Equation 1 is horizontally nondivergent and the horizontal fluid velocity $\mathbf{u} = (u, v)$ has components $u = -\partial\psi/\partial y$ and $v = \partial\psi/\partial x$. Equation 1 is the called the barotropic quasigeostrophic approximation. In the context of plasma physics, Equation 1 is referred to as the Hasegawa-Mima equation (Hasegawa & Mima 1978).

In the case of motion at scales smaller than the Rossby deformation radius R, the effect of the free surface can be discarded. Moreover, on such scales the f-plane approximation is often sufficient. Under the conditions $\beta = 0$ and $R \to \infty$ the barotropic QG equation (Equation 1) becomes the standard equation for two-dimensional (2D) turbulence, where potential and relative vorticity coincide.

In the absence of forcing and dissipation ($F = D = 0$), 2D turbulence admits an infinite number of conserved quantities. Two of them are quadratic invariants, namely the mean kinetic energy $E = 1/8\pi^2 \int (\nabla\psi)^2 \, dx \, dy$, and the mean enstrophy $Z = 1/8\pi^2 \int (\nabla^2\psi)^2 \, dx \, dy$, where we have considered a square domain with size 2π. The simultaneous conservation of energy and enstrophy induces a direct (i.e. from large to small scales) cascade of enstrophy and an inverse (from small to large scales) cascade of kinetic energy (Kraichnan 1967, Leith 1968, Batchelor 1969, Lilly 1972, Kraichnan & Montgomery 1980, Couder 1984, Frisch & Sulem 1984, Herring and McWilliams 1984, Lesieur 1987, Maltrud & Vallis 1991, 1993), at variance with what happens in three dimensions, where enstrophy is not conserved and energy cascades from large to small scales.

The inverse cascade of energy induces important consequences on the dynamics of 2D turbulence. Numerical simulation and laboratory experiments have revealed the presence of strong, long-lived vorticity concentrations that contain most of the energy and the enstrophy of the system and live much longer than their typical eddy turnover time. The first clear evidence of the spontaneous emergence of coherent vortices in 2D turbulence was provided by McWilliams (1984), although indications of this phenomenon can be found in earlier works (e.g. Fornberg 1978, Basdevant et al 1981). The qualitative appearance of 2D turbulence is thus a random, low-energy background turbulent field intermittently punctuated by strong individual vortices and high-vorticity filaments, formed mainly during anelastic vortex-vortex interactions.

In freely decaying turbulence ($F = 0$ and $D \neq 0$), coherent vortices generally form after the time of maximum energy dissipation rate and display a broad distribution of size and circulation. After the first burst of vortex formation, the vortex dynamics is characterized by long-range interactions that can be approximately modeled by point-vortex systems, temporary dipolar pairing between vortices of opposite sign, and strong anelastic interactions between

vortices of the same sign (McWilliams 1984, 1990a, Benzi et al 1986, 1987, Couder & Basdevant 1986, Waugh 1992, Dritschel & Waugh 1992, Dritschel 1995, Dritschel & Zabusky 1996). Moreover, the presence of coherent vortices tends to suppress the turbulent cascades (McWilliams 1990b).

Figure 1*a* shows a typical vorticity field obtained by numerical simulation of Equation 1 with $F = 0$, $\beta = 0$, and $1/R = 0$, starting from an initially random gaussian vorticity field characterized by a narrow band energy spectrum $E(k) = E_0 k^6/(2k_0 + k)^{18}$ and random Fourier phases (McWilliams 1990a). Here $k_0 = 30$ and E_0 is a normalization factor that is fixed by requiring the mean initial energy $E = \int E(k)\,dk = 0.5$. The mean initial enstrophy is $Z = 1100$. Here and in the following we use periodic boundary conditions in a square box with size 2π. For this simulation, a pseudospectral code with standard 2/3 dealiasing and resolution 512^2 grid point has been used (Orszag 1971, Canuto et al 1987). The time integration is performed by a third-order Adams-Bashford scheme and dissipation is provided by a biharmonic term $D = -\nu_2 \nabla^4 \nabla^2 \psi$ with $\nu_2 = 5 \cdot 10^{-8}$. Several works have been devoted to study the statistical properties of the vortex population in freely decaying 2D turbulence and its dependence on numerical resolution, initial conditions, and dissipation scheme (Benzi et al 1987, Brachet et al 1988, Santangelo et al 1989, McWilliams 1990a, Carnevale et al 1991, Dritschel 1993, Weiss & McWilliams 1993, Bartello & Warn 1996). At very late times, for systems with zero average vorticity in periodic or bounded domains the inverse energy cascade and the merging of same-sign vortices lead to the presence of a vortex dipole at the largest scales (Matthaeus et al 1991). This dipole is usually characterized by a very small nonlinearity [i.e. $[\psi, \nabla^2 \psi \approx 0]$] and it decays slowly due to dissipation.

Freely decaying turbulence is not in a state of statistical equilibrium. Whenever a statistically stationary turbulent flow is needed, forcing must balance dissipation in such a way that the total energy and enstrophy of the system do not show any temporal trend. Simulations of forced, statistically stationary barotropic turbulence with coherent vortices have been discussed by Babiano et al (1987a,b, 1990, 1994, 1995), Elhmaidi et al (1993), Legras et al (1988), Ohkitani (1991), Maltrud and Vallis (1991, 1993), Borue (1994), Provenzale et al (1995, 1998). In the following, we consider both freely decaying and forced turbulent flows.

As evident from Figure 1*a*, the general appearance of 2D turbulence is quite complicated. To characterize this complex topology, one can employ a partition of the turbulent field proposed by Okubo (1970) and Weiss (1991) [see also McWilliams (1984), Elhmaidi et al (1993), Larcheveque (1990), Basdevant & Philipovitch (1994), Hua & Klein (1998)]. The Okubo-Weiss criterion is based on considering the evolution equation for the vorticity gradient $\nabla\omega$ in the limit

(a)

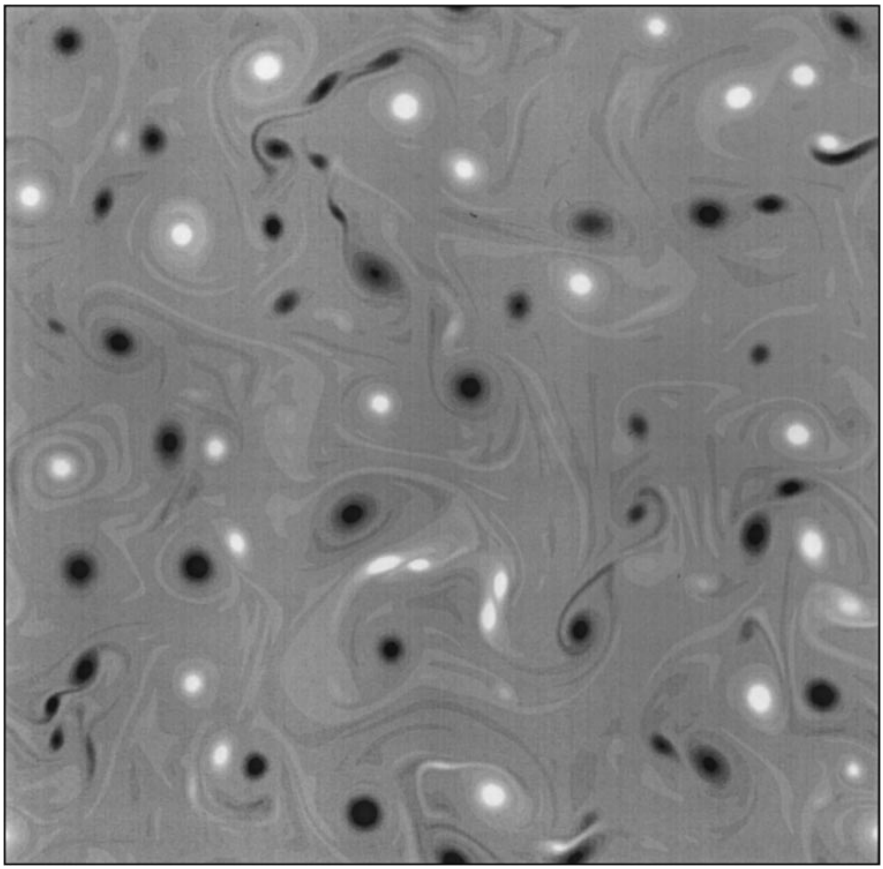

Figure 1 (*a*) Vorticity field from a numerical simulation of freely decaying two-dimensional turbulence with $1/R = \beta = 0$ at time $t = 10$. Initial conditions are provided by a Gaussian random vorticity field with narrow-band energy spectrum, mean initial energy $E = 0.5$, and mean initial enstrophy $Z = 1100$. *Bright* and *dark tones* indicate negative and positive vorticity respectively. (*b*) The field of the Okubo-Weiss parameter Q for the vorticity field shown in Figure 1*a*. *Bright* and *dark tones* indicate negative and positive values of Q, respectively.

of vanishing viscosity; i.e. when vorticity is a Lagrangian invariant. In the incompressible case, this equation reads

$$\frac{D\nabla\omega}{Dt} + [\nabla\psi, \omega] = 0. \tag{3}$$

Under the assumption that vorticity and strain (i.e. spatial velocity derivatives) are slowly varying with respect to the vorticity gradient in a Lagrangian frame, the general solution of Equation 3 is given by a linear combination of the two

(b)

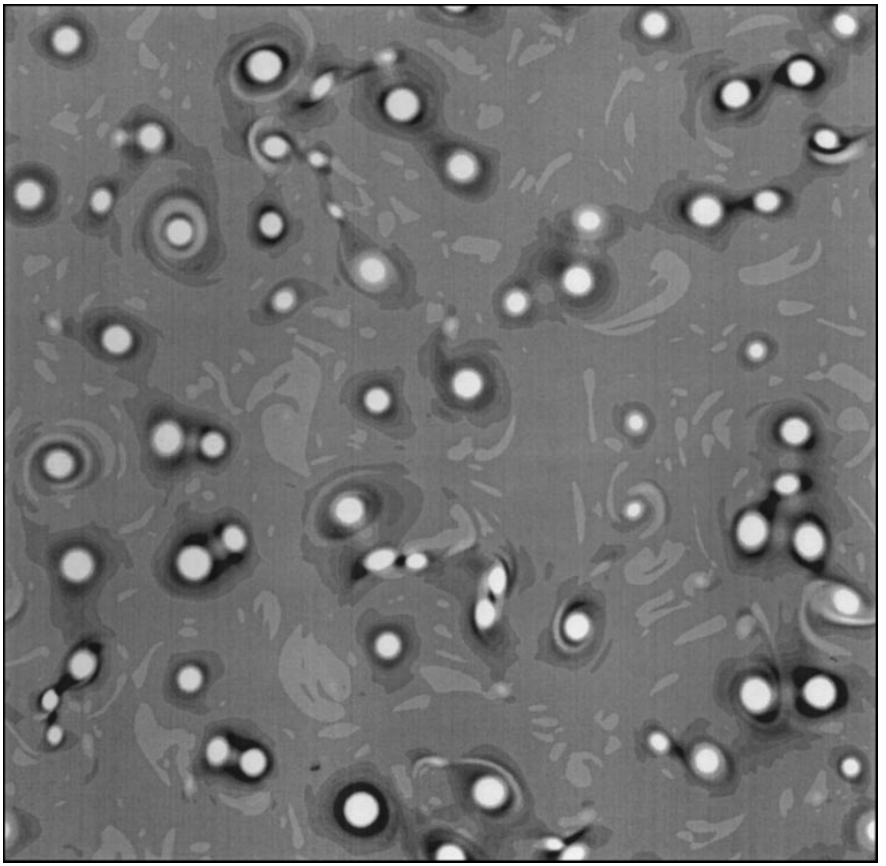

Figure 1 (*Continued*)

elementary solutions

$$\nabla\omega_{\pm} \propto \exp\left(\pm\frac{1}{2}Q^{\frac{1}{2}}t\right) \tag{4}$$

where $Q = Q(x, y, t) = S^2 - \omega^2$. Here

$$S^2 = S_n^2 + S_s^2, S_n = \partial_x u - \partial_y v, S_s = \partial_x v + \partial_y u,$$

where S_n and S_s are the normal and shear components of strain, respectively.

The Okubo-Weiss parameter Q measures the relative contribution of the squared strain S^2 and of the squared vorticity ω^2. Elliptic regions are dominated by rotation and are characterized by $Q < 0$, while hyperbolic regions are

dominated by strain and deformation and are characterized by $Q > 0$. Note that the value of Q defines the behavior of advected particles in the *frozen* field: Regions with $Q > 0$ are characterized by local exponential divergence of nearby particles, while regions with $Q < 0$ are characterized by an approximate constancy of the distance between nearby particles. Of course, this does not bear any direct information on the chaotic or regular nature of the trajectories of advected particles in the evolving field.

Figure 1*b* shows $Q(x, y)$ for the vorticity field of Figure 1*a*. Based on the value of Q, we identify three regions, namely (*a*) vortex cores, which are characterized by strong negative values of Q; (*b*) strain cells surrounding the vortices, which are characterized by large positive values of Q; and (*c*) the background where Q fluctuates between small positive and negative values. Depending on the sign of Q, the background field may be further divided into noncoherent elliptic and hyperbolic patches.

In past years, various authors have discussed the Okubo-Weiss criterion. In particular, Basdevant & Philipovitch (1994) have shown that this criterion is strictly justified only in a small portion of the turbulent field, and Hua & Klein (1998) have proposed an extension of this approach that explicitly takes into account time evolution. On the other hand, the partition of the turbulent field into elliptic and hyperbolic regions has proven to be of value in the study of absolute dispersion of passively advected fluid particles, see e.g. Elhmaidi et al (1993). The use of such a parameterization has led to the identification of the trapping properties of barotropic coherent vortices and to the observation of different transport regimes associated with different regions of the turbulent flow.

Before closing this section, it is useful to briefly discuss the fate of coherent vortices when free surface effects and differential rotation cannot be neglected.

Vortex dynamics for $1/R \neq 0$ and $\beta = 0$ has been discussed by Polvani et al (1989), Larichev & McWilliams (1991), Waugh (1992), Kukharkin et al (1995). The presence of a free surface slows down the inverse cascade at scales larger than R. The interaction between different vortices is shielded at large scales, and the dynamics becomes spatially more localized. At scales smaller than R, the dynamics is basically that of 2D turbulence. Coherent vortices form and grow by merging until they reach a scale of order R. After this stage, the evolution becomes very slow because the different vortices interact only weakly with each other. Figure 2 shows a plot of the vorticity field from a numerical simulation of barotropic turbulence with $R = 0.2$ (one fifth of the domain size) and $\beta = 0$, for the same initial condition of Figure 1. Note the existence of several vortices encapsulated in subdomains with typical size R.

Differential rotation, associated with $\beta \neq 0$, induces more significant effects (e.g. Rhines 1975, 1979, McWilliams 1984, Bartello & Holloway 1991,

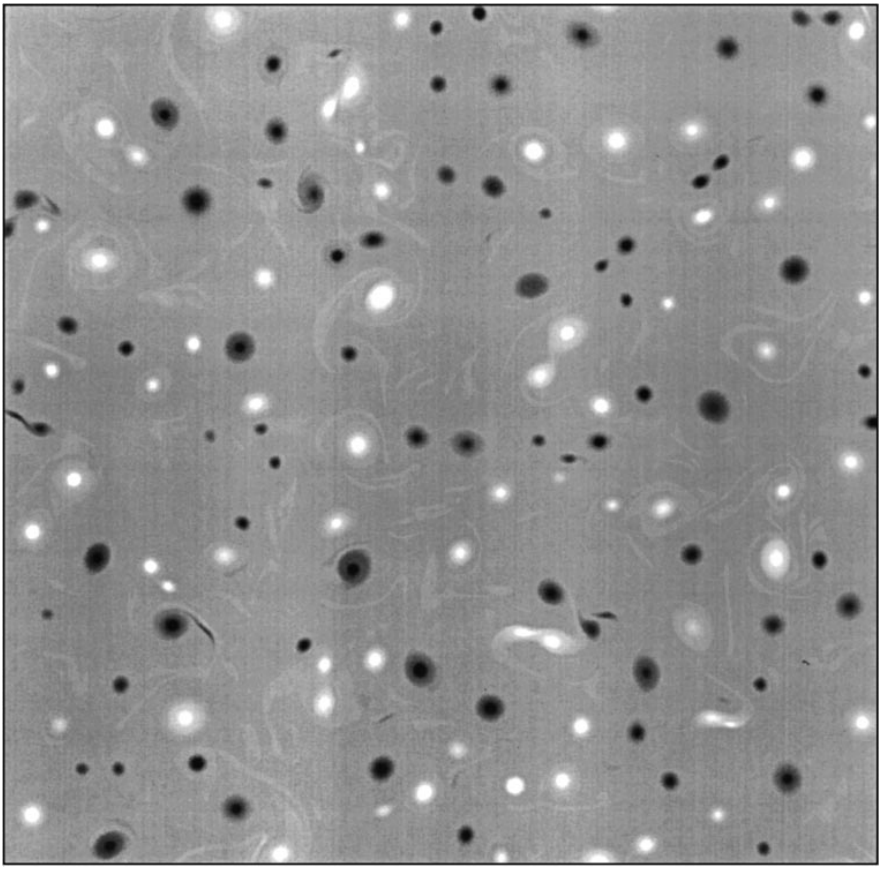

Figure 2 Potential vorticity field from a numerical simulation of freely decaying barotropic turbulence on the *f*-plane with $\beta = 0$ and $R = 0.2$ at $t = 10$. *Bright* and *dark tones* indicate negative and positive vorticity respectively. Same initial conditions of Figure 1*a*.

Maltrud & Vallis 1991, 1993). In particular, the β-term is responsible for the existence of an upper scale $L_\beta = (U/\beta)^{1/2}$, called the Rhines scale, above which the inverse energy cascade is inhibited (Rhines 1975). Here, U is a typical velocity scale which is determined by the dynamics. Above the Rhines scale, Rossby waves dominate the dynamics; usually, coherent vortices cannot grow larger than L_β. Even below the Rhines scale, β-plane vortices live shorter than their *f*-plane counterparts. In general, isolated monopoles on the β-plane emit Rossby waves and undergo zonal and meridional motion (Firing & Beardsley 1976, McWilliams & Flierl 1979, Flierl et al 1983, Flierl 1987,

Sutyrin & Flierl 1994, Sutyrin et al 1994, Reznik & Dewar 1994, Korotaev & Fedotov 1994, Llewellyn-Smith 1997, Morel & McWilliams 1997, Sutyrin & Morel 1997). Nevertheless, even on the β-plane coherent vortices still form and exist for relatively long times and can induce significant effects on transport, as discussed in the next section. Figure 3 shows the vorticity field obtained by numerical simulation of freely-decaying turbulence with $1/R = 0$ and $\beta = 10$. This picture illustrates the coexistence of Rossby waves and coherent vortices, which is typical of β-plane turbulence.

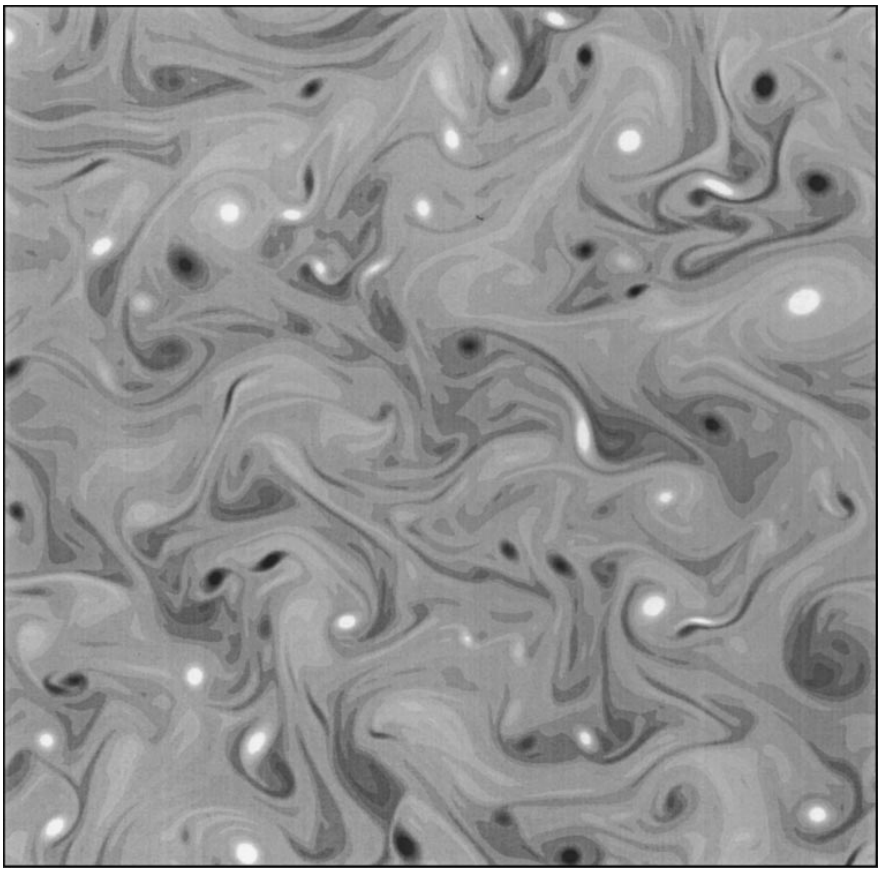

Figure 3 Relative vorticity field from a numerical simulation of freely decaying turbulence on the β-plane at time $t = 10$. Here, $\beta = 10$ and $1/R = 0$. *Bright* and *dark tones* indicate negative and positive vorticity respectively. Same initial conditions of Figure 1*a*.

3. *Particle Advection in Turbulent Flows*

The equations of motion for passive, point-like Lagrangian particles having vanishing inertia with respect to the advecting fluid are obtained by equating the Lagrangian velocity to the Eulerian fluid velocity at the particle position, i.e.

$$\frac{d\mathbf{x}}{dt} = \mathbf{V}(t) = \mathbf{u}(\mathbf{x}, t), \tag{5}$$

where $\mathbf{x}(t) = [x(t), y(t)]$ is the particle position at time t, $\mathbf{V}(t)$ is its Lagrangian velocity, and $\mathbf{u}(\mathbf{x}, t)$ is the Eulerian velocity at point $\mathbf{x}$ and time t.

For two-dimensional incompressible flows, such as those discussed in the previous section, the Eulerian velocity may be expressed in terms of a stream function $\psi(x, y, t)$. In this case Equation 5 becomes

$$\frac{dx}{dt} = -\frac{\partial \psi}{\partial y}; \quad \frac{dy}{dt} = \frac{\partial \psi}{\partial x}. \tag{6}$$

Equation 6 formally defines a Hamiltonian system with one degree of freedom, described by the canonically conjugate variables x and y. Here, the stream function ψ plays the role of the Hamiltonian and the phase space of the system is the physical plane (x, y), see e.g. Ottino (1989). For stationary stream functions, Equation 6 is integrable, the particles follow the streamlines, and all particle trajectories are regular. When the stream function is time-dependent (e.g. periodic in time), the system becomes nonintegrable. In this case, chaotic particle trajectories are expected and the Lagrangian motion may become highly irregular even if the Eulerian dynamics is simple. This type of behavior, known as chaotic advection, has been studied by many authors [see e.g. the reviews by Ottino (1989, 1990), Crisanti et al (1991), Wiggins (1992)].

When particle trajectories are irregular, statistical quantities are needed to characterize the Lagrangian properties. The maximum Lagrangian Lyapunov exponent provides a measure of the degree of chaoticity of a trajectory. Given two infinitesimally close trajectories $\mathbf{x}_1(t)$ and $\mathbf{x}_2(t) = \mathbf{x}_1(t) + \delta\mathbf{x}(t)$, solutions of Equation 6, in the limit $|\delta\mathbf{x}| \to 0$ the time evolution of the separation vector $\delta\mathbf{x}$ is given by the linearized equation

$$\frac{d\delta\mathbf{x}}{dt} = \frac{\partial(u, v)}{\partial(x, y)}\delta\mathbf{x}, \tag{7}$$

where $\partial(u, v)/\partial(x, y)$ is the velocity Jacobian matrix computed along $x, (t)$. The maximum Lagrangian Lyapunov exponent λ_L is then defined as

$$\lambda_L = \lim_{t\to\infty} \Lambda_L(t) = \lim_{t\to\infty} \lim_{|\delta\mathbf{x}(0)|\to 0} \frac{1}{t} \log \frac{|\delta\mathbf{x}(t)|}{|\delta\mathbf{x}(0)|}. \tag{8}$$

For Hamiltonian systems, a regular and predictable Lagrangian behavior is associated with a value $\lambda_L = 0$, while chaotic and unpredictable particle trajectories are associated with $\lambda_L > 0$.

The relevant information is contained in the time-dependence of Λ_L. Regular motion induces an ever-decreasing value of Λ_L, while chaotic dynamics induces a convergence of Λ_L to a finite positive value, giving an estimate of λ_L. Note, also, that the maximum Lagrangian Lyapunov exponent is based on a time average along a single trajectory, and must be computed for each fluid particle. From a practical point of view, there are various algorithms that provide an approximation to $\Lambda_L(t)$ from the knowledge of the equations of motion, see e.g. Benettin et al (1976, 1980), Eckmann & Ruelle (1985). On some occasions, local Lyapunov exponents (also called Finite Time Lyapunov Exponents, FTLE) have been introduced (e.g. Pierrehumbert 1991a, Pierrehumbert & Yang 1993). These are obtained by taking a finite (and usually small) value for t in Equation 8, with the aim of generating a map of the FTLE as a function of the starting position of the particles. Although useful under several circumstances, we shall not use the FTLE approach here.

Further information on particle advection is provided by the study of absolute and relative dispersion. Both these concepts are based on averaging over an ensemble of advected particles, rather than on averaging over time as for the Lyapunov exponents. Absolute dispersion (also called single-particle dispersion) provides a measure of the mean square displacement of individual particles at time t, and it is defined as

$$A^2(t;t_0) = \langle |\mathbf{x}_i(t) - \mathbf{x}_i(t_0)|^2 \rangle = \frac{1}{N} \sum_{i=1}^{N} |\mathbf{x}_i(t) - \mathbf{x}_i(t_0)|^2, \tag{9}$$

where $\langle \cdots \rangle$ indicates average over the particle ensemble, $\mathbf{x}_i(t)$ is the position of the i-th particle at time t, t_0 is the time at which particles have been released, and N is the total number of particles in the ensemble. For statistically stationary flows, single-particle dispersion depends only on $t - t_0$.

The definition of the particle ensemble requires some care. In principle, particles should be released at the same spatial position, in different realizations of the same turbulent flow (Monin & Yaglom 1971). In most practical applications, however, particles are seeded in different spatial positions of the same realization of the flow. The two definitions are compatible if the flow is spatially homogeneous and the initial particle separation is larger than the spatial correlation scale of the flow.

For homogeneous flows, the starting positions $\mathbf{x}_i(t_0)$ of the particles are not important, but they may become so when the flow displays spatial inhomogeneities. In this case, conditional averages can be used (Elhmaidi et al 1993).

Further complications arise when dealing with anisotropic flows, such as on the β-plane. In this case, dispersion along x and y can be different, and the two components of the squared displacement must be considered separately.

Relative dispersion is defined as the mean square displacement at time t between a pair of initially nearby particles. This is given by

$$D^2(t; t_0, d_0) = \frac{1}{N/2} \sum_{i=1,3,5,\ldots} |\mathbf{x}_i(t) - \mathbf{x}_{i+1}(t)|^2, \tag{10}$$

where $N/2$ is the number of particle pairs and d_0 is the initial distance between a particle pair. In the limit of $d_0 \to 0$, one may relate relative dispersion to the ensemble average of the largest Lyapunov exponent.

Armed with these statistical tools, we may now study the transport properties of barotropic vortices.

4. *Transport by Isolated Vortex Structures*

A coherent vortex is a region inside closed vorticity isolines, which keeps its identity for times much longer than the local eddy turnover time T_Z, defined as $T_Z \approx Z^{-1/2}$, where Z is the local average enstrophy. The core of a coherent vortex is the region where $Q \ll 0$, and it is bounded by the isoline $Q = 0$.

From a Lagrangian viewpoint, there is a significant difference between a vortex core and the external field. Figure 4 shows the evolved distribution of 2000 advected particles initially seeded on a straight line from the center of the simulation domain to its edge, in a freely decaying, initially perturbed vortex with $1/R = 0$ on the f-plane. The vortex center (x_0, y_0) coincides with the center of the simulation domain and the initial vorticity profile is given by $\omega(r, \phi, t = 0) = \omega_0 \exp\{-[r/\sigma(\phi)]^4/2\}$, where $r = [(x-x_0)^2 + (y-y_0)^2]^{1/2}$, $\phi = \arctan[(y - y_0)/(x - x_0)]$, and $\sigma(\phi) = \sigma_0[1 + \epsilon \cos(m\phi)]$. Here $m = 3$ is the azimuthal wavenumber, $\epsilon = 0.3$, and $\sigma_0 = \pi/2$. The value of ω_0 is fixed by requiring the mean initial energy of the vortex to be $E = 0.5$. The mean initial enstrophy is $Z = 0.6$. During the free evolution, the vortex tends toward a circular shape, emitting vorticity filaments and interacting with its images in the periodic domain.

In the vortex core, initially nearby particles remain close to each other, gently undergoing linear azimuthal dispersion because of differential rotation inside the vortex. Outside the vortex, particles are rapidly dispersed and they soon display an irregular distribution. Here, one observes exponential stretching of material lines and a corresponding exponential divergence of nearby particles. Analogous results are obtained for a finite Rossby deformation radius.

The behavior of particles inside and outside the vortex can be quantified by considering the radial relative dispersion between pairs of nearby particles. Radial relative dispersion can be defined as the radial component of the relative

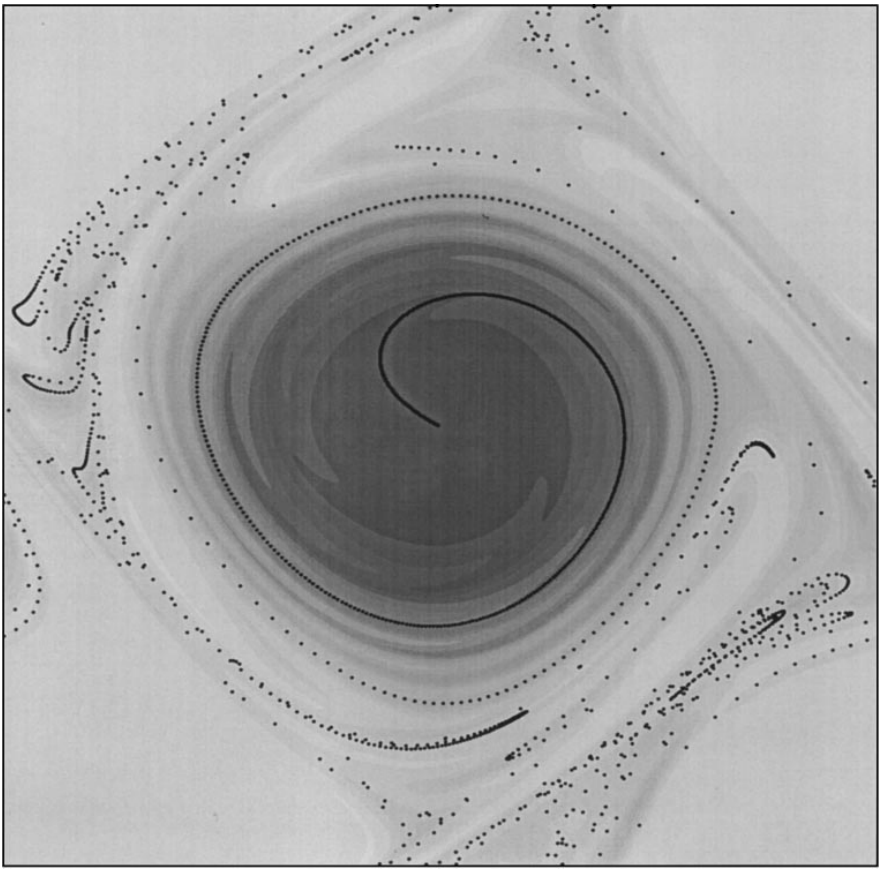

Figure 4 Distribution of 2000 passively advected particles at $t = 20$. Particles are seeded at $t = 0$ on a radial line in an azimuthally perturbed cyclonic vortex undergoing freely decaying two-dimensional dynamics with $1/R = \beta = 0$. The mean initial vortex energy is $E = 0.5$ and the enstrophy is $Z = 0.6$. The *shading* represents the evolved vorticity field.

dispersion $D^2(t)$ given by Equation 10, the origin of the polar coordinate system coinciding with the vortex center. Provenzale et al (1998) have shown that particles in a vortex core display an almost null radial relative dispersion and a linear azimuthal dispersion, while particles outside undergo strong radial relative dispersion.

The above results indicate that particle motion is regular inside coherent vortices. The lack of Lagrangian chaoticity in the vortices of 2D turbulence has been discussed by Babiano et al (1994), who have shown that the maximum

Lagrangian Lyapunov exponent converges toward zero inside vortex cores. Outside vortices, particle trajectories in 2D turbulence are generally chaotic and have a positive maximum Lagrangian Lyapunov exponent. In a sense, coherent vortices in barotropic turbulence can be defined as islands of regular Lagrangian dynamics in a chaotic background. It is interesting to note that these regular islands are not fixed in space and time, as they wander chaotically in the turbulent field and have finite lifetime. The lack of chaoticity in the vortices indicates that Lagrangian mixing is very weak inside vortices, and it is achieved only on diffusive time scales by the combined action of viscosity and differential rotation inside the vortex.

An important property of coherent barotropic vortices is their impermeability to inward and outward particle fluxes (Elhmaidi et al 1993, Babiano et al 1994; see also Dewar & Flierl 1985). Figure 5 shows the distribution of two ensembles of passive tracers seeded respectively inside and outside a coherent vortex in freely decaying 2D turbulence ($\beta = 0$ and $1/R = 0$), using the same initial conditions of Figure 1*a*. Particles are seeded at $t = 10$ when the coherent vortices are already present. At the seeding time, the mean kinetic energy of the Eulerian field is $E = 0.35$ and the mean enstrophy is $Z = 20$. The system is then integrated up to a time $t = 42$. The particles inside the vortices remain there, while those seeded outside spread in the background turbulent field, without entering any vortex core. Analogous results have been discussed by Elhmaidi et al (1993) for forced 2D turbulence. In this latter case, particles are ejected from vortex cores only during strong vortex-vortex interactions, and no particles enter the cores of existing vortices. In forced turbulence, vortices are continuosly (albeit slowly) generated and the only possibility for a particle to enter a vortex core is to be captured by a newly forming vortex during the generation process. Thus, in forced turbulence the particle distribution becomes homogeneous on a very long time scale, which is determined by the typical lifetime of the vortices rather than by the eddy turnover time of the individual vortices. In stationary or oscillatory flows, closed streamlines delay homogeneization of passive scalars, as shown by Rhines & Young (1983). The above results show that even in turbulent flows the presence of chaotically moving regular islands associated with the coherent vortices leads to a similar delay of homogeneization.

The presence of a β term does not destroy the trapping properties of coherent vortices. Although vortices may be short-lived because of emission of waves and vorticity filaments, below the Rhines scale vortex cores still act as trapping islands as long as they exist. Figure 6 shows the distribution at $t = 20$ of an ensemble of particles initially seeded inside a vortex core, in freely decaying barotropic turbulence on the β-plane. For this simulation, $\beta = 10$ and $1/R = 0$. Particles are seeded inside a randomly selected vortex at time $t = 10$, when

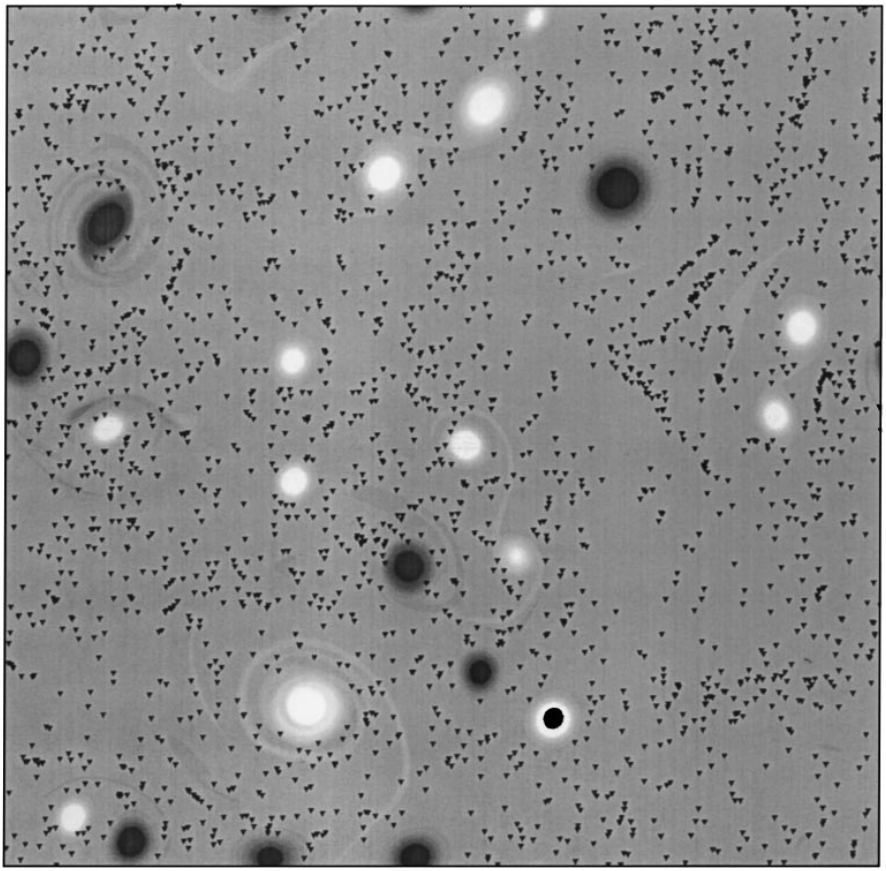

Figure 5 Evolved distribution of two ensembles of passive particles that were initially seeded inside a vortex core and in the background field in freely decaying two-dimensional turbulence. Particles seeded in the vortex remained there during the turbulent evolution and can be seen inside the vortex in the lower right portion of the domain. Particles seeded in the background (*small solid triangles*) do not enter vortex cores and spread in the background turbulent field. In this figure, *bright* and *dark tones* indicate positive and negative vorticity respectively.

the turbulent field is already organized in coherent vortices and the mean kinetic energy is $E = 0.35$. Most of the particles are trapped in the vortex during its entire lifetime, being released only when the vortex is destroyed at $t \approx 20$.

Particle trapping inside coherent monopoles on the β-plane can have important consequences on the overall transport of passive tracers. In the presence of a β term, transport in the meridional direction (i.e., parallel to the direction along which the Coriolis parameter varies) is generally inhibited. Rossby waves tend to move passive constituents mainly along the zonal direction, and

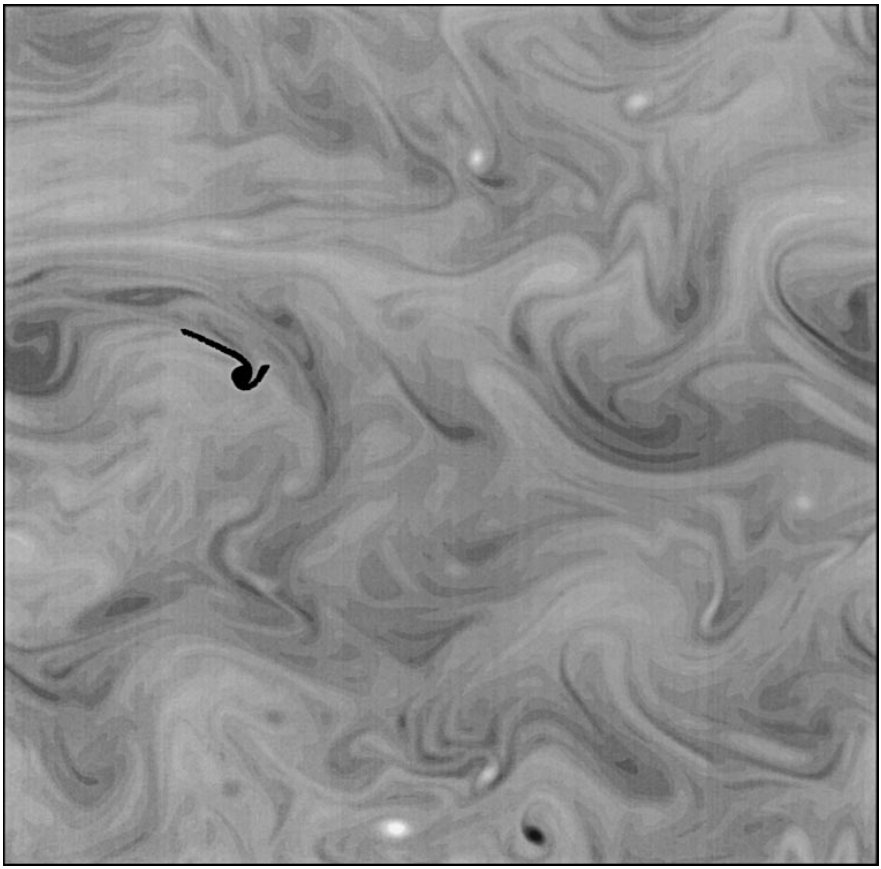

Figure 6 Evolved distribution of an ensemble of passive particles that were initially seeded inside a vortex core in freely decaying turbulence on the β-plane. Here $\beta = 10$. Most of the particles have been trapped in the vortex for its whole lifetime and are released only after the disruption of the vortex itself. *Bright* and *dark tones* indicate negative and positive vorticity respectively.

a marked asymmetry between zonal and meridional transport is observed (e.g. Pierrehumbert 1991b). By contrast, coherent vortices may have a significant meridional component in their motion. Passive tracers trapped inside vortices are also displaced meridionally, and, when the vortex finally disappears, are released at a different latitude with respect to their original location. Trapping of passive tracers inside coherent monopoles can thus provide a mechanism of meridional mixing on the β-plane.

The trapping properties of coherent vortices can be understood by noting that the vortices have a strong vorticity gradient at their edge, which separates the

rotation-dominated core from the strain-dominated region just outside. In two-dimensional turbulence, relative vorticity is a material invariant when forcing and dissipation are absent. In QG turbulence, the same happens for potential vorticity. In the presence of forcing, dissipation, or weak three-dimensional effects, vorticity is not exactly conserved and fluid particles can cross vorticity isolines. If the perturbing effects are weak, however, particles can change their vorticity only slightly. Thus, regions of uniform or gently variable vorticity are easily crossed by fluid particles while regions of large vorticity gradient act as transport barriers, since the fluid particles cannot change their vorticity enough to cross them. This criterion, discussed by McIntyre (1989) in the context of polar vortex dynamics, can be applied also to the case of barotropic vortices.

The edge of a coherent vortex may thus be defined as the isoline of maximum vorticity gradient closer to the vortex center. Previously, we have defined the vortex edge as the inner isoline where $Q = 0$. Close to this isoline, the kinetic energy and the vorticity gradient reach their maximum. Although the isolines of maximum kinetic energy, maximum vorticity gradient, and $Q = 0$ do not necessarily coincide, in general they provide three consistent definitions of the vortex edge (Paparella et al 1997).

A striking geophysical example of the impermeability of coherent vortices is provided by the polar stratospheric vortex (Paparella et al 1997). The polar vortex is a strong, quasistationary stratospheric wind system that fully develops during winter. In the Southern hemisphere, the stratospheric polar vortex is particularly stable, and it is characterized by a limited exchange between the air masses inside and outside it.

Figure 7 (from Paparella et al 1997) shows the simulated trajectories of 30 isopycnal balloons initially released at 292°E and 63°S on the isopycnal surface at $\rho = 0.0938$ kg/m^3 (corresponding to an approximate height of 20 km). The balloons were released every two days starting on August 1st, 1993, and their trajectories were numerically simulated using the ECMWF meteorological wind fields for the period under study and a dedicated Lagrangian advection scheme. From Figure 7, it is clear that the balloons, which were initially released just outside the edge of the polar vortex, did not enter the vortex due to the strong impermeability of the vortex edge. Analogously, balloons released inside the vortex tended to stay inside, and spread out only at the end of the Southern polar winter when the vortex weakened. Analogous results are obtained for passive particle motion on isentropic surfaces.

5. *Absolute Dispersion in Vortex-Dominated Flows*

Having discussed how individual coherent vortices affect particle transport, we may now concentrate on the Lagrangian behavior of flows dominated by the

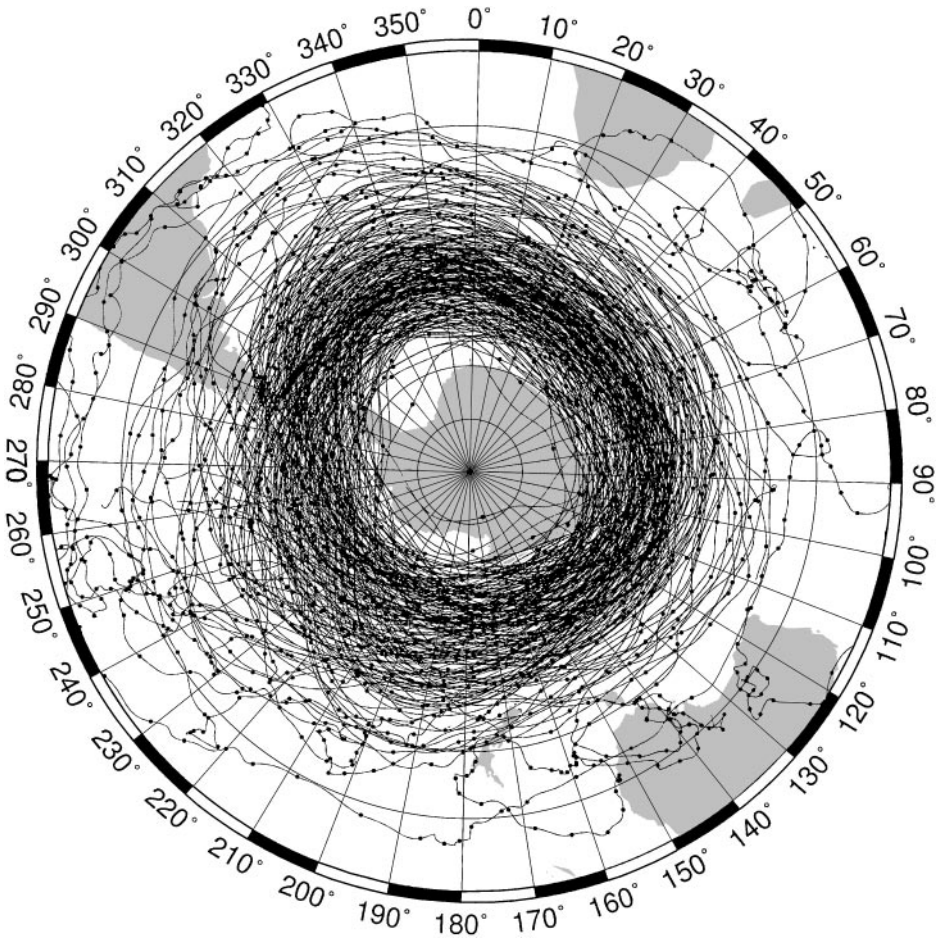

Figure 7 Simulated trajectories of 30 isopycnal balloons in the southern polar stratosphere. The balloons are initially released at 292°E and 63°S on the isopycnal surface at $\rho = 0.0938$ kg/m^3, corresponding to an approximate height of 20 km. The balloons were released every two days starting on August 1st, 1993, and their trajectories were numerically simulated using the ECMWF meteorological wind fields (from Paparella et al 1997).

presence of several vortices and on the properties of absolute dispersion in 2D turbulence.

Absolute (or single-particle) dispersion is defined by Equation 9. In homogeneous and isotropic 2D turbulence, particle trajectories are differentiable at short times and absolute dispersion takes a ballistic form, $A^2(t) = 2\langle E\rangle t^2$, where the initial time is $t_0 = 0$ and $\langle E\rangle$ is the average kinetic energy of the particle ensemble during the time interval $[0, t]$. At large times, particle motion becomes analogous to a random walk, and absolute dispersion takes the standard Brownian form $A^2(t) = 2Kt$, where K is the dispersion coefficient (Taylor 1921, Monin & Yaglom 1971).

The meaning of "short" and "large" times for particle dispersion is determined by the value of the Lagrangian integral time T_L. This quantity can be obtained by a time average over particle trajectories. We define the ensemble-averaged Lagrangian velocity autocorrelation as

$$R(\tau) = \lim_{T\to\infty} \frac{1}{T}\left\langle \frac{1}{\sigma_i^2}\int_0^T \mathbf{V}_i'(t)\cdot\mathbf{V}_i'(t+\tau)\,dt \right\rangle \tag{11}$$

where $\langle\cdots\rangle$ indicates average over the particle ensemble, $\mathbf{V}_i'(t) = \mathbf{V}_i(t) - \bar{\mathbf{V}}_i$ is the Lagrangian velocity fluctuation of the i-th particle, $\mathbf{V}_i$ is the average Lagrangian velocity, and σ_i^2 is the velocity variance. The average energy spectrum of the particles is given by

$$P(\nu) = 2\int_0^\infty R(\tau)\cos(2\pi\nu\tau)\,d\tau, \tag{12}$$

where ν is frequency. The average Lagrangian integral time is then defined as

$$T_L = \int_0^\infty R(\tau)\,d\tau = \frac{1}{2}P(0). \tag{13}$$

Thus, short times are those which are much smaller than the average Lagrangian integral time T_L, while long times are much longer than T_L.

The ballistic and Brownian regimes, respectively at $t \ll T_L$ and $t \gg T_L$, have a rather general nature. In practical situations, however, T_L is often comparable with the time scale of interest in the dynamics, e.g. T_L is a few days for mesoscale ocean flows. In addition, often the large-time Brownian regime cannot be observed because of large-scale Eulerian inhomogeneities. Under these conditions, it becomes important to understand dispersion on times comparable with T_L, in order to provide appropriate models for the parameterization of transport. Anomalous diffusion (i.e. neither ballistic nor Brownian) has been experimentally observed in two-dimensional chaotic advection (Solomon et al 1993, 1994).

The work of Elhmaidi et al (1993) has considered the properties of absolute dispersion in forced and dissipated 2D turbulence, focusing on intermediate

times. In this work, forcing is obtained by keeping fixed the power spectrum at a selected wavenumber, simulating the contact of the turbulent flow with an external energy and enstrophy reservoir. Dissipation is introduced at both small and large scales, in order to dissipate the energy piled up by the inverse cascade.

One series of runs has resolution 128^*128 grid points in the periodic square domain with size 2π. Large-scale forcing is fixed at the wavenumber $k_F = (10, 0)$. An initial random field is evolved until statistical equilibrium is reached and vortices form; passive particles are seeded into the turbulent flow only after this moment. At equilibrium, the average Eulerian integral time scale is $T_E = 0.14$ and the average Lagrangian integral time is $T_L = 0.035$. At variance with what happens for free decay, in this type of forced turbulence the vortices have a narrow distribution of size, centered on the forcing scale.

The study of absolute dispersion has allowed Elhmaidi et al (1993) to identify the existence of a regime of anomalous dispersion at intermediate times. By using conditional averages over the particle ensemble, it has been shown that absolute dispersion in strain-dominated regions where $Q > 0$ is characterized by the approximate power-law behavior

$$A^2(t) \propto t^{5/4}, \tag{14}$$

at times between approximately $2T_L$ and $30T_L$. This anomalous dispersion regime is related to motion in the strain-dominated cells that surround coherent vortices and in the hyperbolic patches of the turbulent background.

A similar intermediate regime of anomalous dispersion has been detected, although indirectly, in the Lagrangian motion of ocean subsurface floats (Rupolo et al 1996). In a reanalysis of the historical data set of SOFAR floats in the western North Atlantic (Richardson et al 1981, Owens 1991), Rupolo et al (1996) have shown that float trajectories with stationary velocity time series possess a kinetic energy spectrum with a generic shape, when the frequency and the spectrum of each trajectory are rescaled by the Lagrangian integral time T_i of the individual trajectory considered, $\hat{P}_i(\hat{\nu}) = P_i(\nu T_i)/T_i$. Note that the Lagrangian integral times are well-defined because only trajectories with stationary velocities have been considered. In this data set, T_i ranges between about three and ten days.

The average adimensional spectrum $\hat{P}(\hat{\nu}) = \langle \hat{P}_i(\hat{\nu}) \rangle$ has been shown to be best-fitted by a three-component function. The best-fit shape is characterized by (*a*) a flat plateau at low frequencies, $\hat{\nu} < 1/30$, associated with the stationarity of the velocity record, (*b*) a very steep slope at high frequencies, $\hat{\nu} > 1/3$, which indicates that Lagrangian accelerations are convergent for the data set considered, and (*c*) an intermediate regime that is approximately fitted by a power law $\hat{P} \propto \hat{\nu}^{-0.25}$. The intermediate regime is particularly visible in the spectra of floats sampling high-energy regions near jet meanders and isolated

vortices. Note that frequencies are given in units of the Lagrangian integral time.

To see the link with absolute dispersion, one has to define the structure function,

$$S_i(\tau) = \left\{ \left| \mathbf{x}_i'(t+\tau) - \mathbf{x}_i'(t) \right|^2 \right\}_t, \tag{15}$$

where $\mathbf{x}_i'(t) = \mathbf{x}_i(t) - \bar{\mathbf{V}}_i t$ is the linearly detrended position time series of the i-th float and the symbol $\{\cdots\}_t$ denotes average over time t. The adimensional structure function is given by $\hat{S}_i(\hat{\tau}) = S_i(\tau/T_i)/(\sigma_i^2 T_i^2)$, where σ_i^2 and T_i are the velocity variance and Lagrangian integral time of the individual trajectory considered.

The ensemble-averaged structure function $\hat{S}(\hat{\tau}) = \langle \hat{S}_i(\hat{\tau}) \rangle$ is equivalent to the absolute dispersion $A^2(\tau)$ with an additional average over the initial dispersion time t. $\hat{S}(\hat{\tau})$ is related to the power spectrum by

$$\hat{S}(\hat{\tau}) = \frac{8}{4\pi^2} \int_0^\infty \frac{\hat{P}(\hat{\nu})}{\hat{\nu}^2} \sin^2(\pi \hat{\nu} \tau)\, d\hat{\nu}. \tag{16}$$

From Equation 16, one sees that a power-law behavior of the average spectrum, $\hat{P} \propto \hat{\nu}^{-\alpha}$, corresponds to a power-law behavior of the structure function, $\hat{S} \propto \tau^{1+\alpha}$. Thus, the value $\alpha = 0.25$ observed for float trajectories is consistent with the absolute dispersion $A^2 \propto t^{5/4}$ observed for strain-dominated regions in 2D turbulence, provided we can identify the structure function with the ensemble absolute dispersion and that the extent of the power-law region in the spectrum is not too small to be masked by the side regimes. Note also that the extent of the intermediate regime, between about $3T_L$ and $30T_L$, is consistent in the two cases.

The results on anomalous dispersion reported above are intriguing and are worth further study. For example, it is unsatisfactory that there is no theoretical explanation of the intermediate regime of anomalous dispersion. In particular, it would be interesting to determine whether the observed approximate power-law behavior is produced by a truly self-similar dynamics or it is generated by other mechanisms, such as a superposition of a small number of dispersion processes with different characteristic times (Artale et al 1997). It would also be of interest to determine the dependence (if any) of the anomalous behavior on the forcing mechanism, on the presence of a free surface ($1/R \neq 0$), and on the β-term. If anomalous dispersion at intermediate times will prove to be a robust property of vortex-dominated turbulent flows, it will then become necessary to take it into account when parameterizing sub-grid mesoscale dynamics. Simple eddy diffusion approaches—which rely upon the presence of a Brownian dispersion regime—cannot represent this process.

6. *Advection in Point-Vortex Systems*

Systems of point vortices represent an extreme form of vortex-dominated flows. Here, vorticity is concentrated in point-like singularities that move because of their mutual advection, and the fluid between the singularities is completely passive (Kirchhoff 1876) [see Aref (1983) for a review]. Point vortices have been shown to mimic the behavior of the extended vortices of 2D turbulence for limited times (Benzi et al 1987), their main drawback being the lack of anelastic vortex-vortex interactions and of vortex merging. Attempts to extend the dynamics of point vortices to include vortex merging have been discussed by Carnevale et al (1991), Benzi et al (1992), Weiss & McWilliams (1993) and Riccardi et al (1995). In past years, several works have been devoted to the study of passive particle advection in point vortex systems (e.g. Aref & Pomphrey 1980, Aref et al 1989, Rom-Kedar et al 1990, Meleshko et al 1992, Babiano et al 1994, Carnevale & Kloosterziel 1994, Velasco Fuentes 1994, Pentek et al 1995, Velasco Fuentes et al 1995, Boffetta et al 1996, Kuznetsov & Zaslavsky 1998, Carena et al 1998, Weiss et al 1998). Here, we briefly review some of these results.

Formally, point vortices are singular solutions of two-dimensional Euler equations. The equations of motion for point vortices can be obtained by supposing the existence of a singular vorticity field

$$\omega(\mathbf{x}, t) = \sum_{i=1}^{N} \Gamma_i \delta[\mathbf{x} - \mathbf{x}_i(t)], \tag{17}$$

where N is the number of vortices, Γ_i is the constant circulation of the i-th vortex and $\mathbf{x}_i(t) = [x_i(t), y_i(t)]$ is its position at time t.

By substituting Equation 17 into the 2D Euler equations [equivalent to Equation 1 with $\beta = 1/R = F = D = 0$], one obtains the equations of motion in the non-canonical Hamiltonian form

$$\Gamma_i \frac{dx_i}{dt} = +\frac{\partial H}{\partial y_i}, \qquad \Gamma_i \frac{dy_i}{dt} = -\frac{\partial H}{\partial x_i}, \tag{18}$$

where H is the Hamiltonian

$$H(\{\mathbf{x}_i\}) = -\sum_{i \neq j} \frac{\Gamma_i \Gamma_j}{2} G(\mathbf{x}_i, \mathbf{x}_j), \tag{19}$$

and the form of the Green function G depends on the boundary conditions.

The motion of N vortices is described by an Hamiltonian system with N degrees of freedom ($2N$ dimensions in phase space). If the system has N_0 independent conserved quantities, the motion of $N \leq N_0$ vortices is regular and the maximum Lyapunov exponent in the $2N$-dimensional phase space is

zero. The motion of $N > N_0$ point vortices is in general chaotic, with a positive maximum Lyapunov exponent.

For a periodic domain with size 2π the Green function takes the form

$$G(\mathbf{x}_i, \mathbf{x}_j) = \sum_{m=-\infty}^{\infty} \ln\left(\frac{\cosh(x_i - x_j - 2\pi m) - \cos(y_i - y_j)}{\cosh(2\pi m)}\right) - \frac{(x_i - x_j)^2}{2\pi}. \quad (20)$$

The function G can be shown to be periodic in x and y, and invariant under the transformation $x \rightleftharpoons y$. The dynamics on the periodic domain has two invariants other than the energy, namely, the components of the linear momentum $P_x = \sum_{i=1}^{N} \Gamma_i y_i$ and $P_y = \sum_{i=1}^{N} \Gamma_i x_i$. Angular momentum is not an invariant because the periodic boundary conditions break rotational symmetry. The invariants P_x and P_y are independent only if the total circulation $\sum_i \Gamma_i$ is zero (Aref 1983).

Passively advected particles are easily incorporated into point-vortex systems as zero-circulation vortices. A vortex with zero circulation, $\Gamma_i = 0$, is advected by the other vortices but it does not affect their motion. The study of passive particle advection in point vortex systems has shown that each vortex is surrounded by a region where passive particles are trapped for extremely long times, analogously to what happens in the cores of extended vortices (Babiano et al 1994, Carena et al 1998). Figure 8 shows the distribution, at four different times, of 1000 passive particles initially seeded around a vortex in a system composed of ten point vortices on the periodic domain. There are five positive and five negative vortices and the total circulation of the system, $\sum_i \Gamma_i$, is zero. The circulation of each vortex is $|\Gamma_i| \approx 3$. Although some of the particles rapidly detach from the vortex, there is an inner island where the particles are trapped for a long time. Similar trapping islands exist around the other vortices.

The size of the trapping islands is determined by the closest encounter between a pair of vortices. For same-sign vortices on the infinite plane, the joint conservation of energy and angular momentum imposes the existence of a minimum distance between the vortices. As a consequence, the trapping islands have a finite size, which is approximately half the minimum distance between the vortices themselves, that is, the minimum distance to the nearest hyperbolic point (Babiano et al 1994). Numerical simulation of vortex motion on the infinite plane has shown that the trapping islands keep their identity and size for extremely long times. I have integrated the motion of a passive particle in an island around a chaotically moving vortex for more than 10^8 particle rotations without observing any significant increase of its distance from the vortex. This

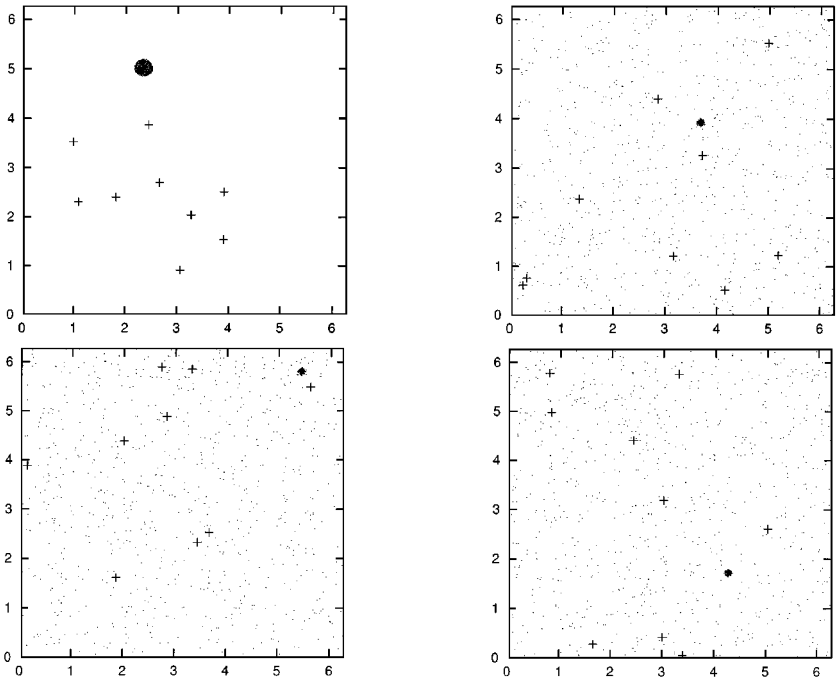

Figure 8 Distribution of vortices (*crosses*) and of 1,000 passively advected impurities (*dots*) in a system of five positive and five negative point vortices on the periodic domain at times $t = 0, 10, 30, 50$. The particles were initially seeded close to one of the vortices. The particles closer to the vortex are trapped in an island of regular Lagrangian dynamics, which moves with the vortex.

behavior suggests an asymptotic nature of the islands around point vortices on the infinite domain.

Particles trapped in the islands around the vortices are characterized by regular Lagrangian motion, analogously to what has been observed for particles in the vortex cores of 2D turbulence. In these islands, the maximum Lagrangian Lyapunov exponent of the passive particles converges to zero even if the vortices move chaotically (Babiano et al 1994). The nature of the regular islands for quasiperiodic vortex motion has been studied by Boffetta et al (1996) for the motion of two vortices in a circular domain and by Kuznetsov & Zaslavsky (1998) for three vortices on the infinite plane.

On the periodic domain, vortices can get closer and closer to each other, and the trapping islands have a size that can slowly shrink in time. However, owing to the rarity of very close encounters between vortices, the islands can still survive for long times.

The Lagrangian dynamics of systems of a large number of positive and negative point vortices on the periodic domain has been studied in detail by Weiss et al (1998). This work has shown that the Lagrangian velocities generated by an ensemble of N vortices are characterized by a probability density function (PDF) with a Gaussian core and power-law tails [see also Min et al (1996) for a study of the velocity PDF of point vortices on the infinite plane]. The high-velocity tails in the PDF disappear, because of central limit theorem, for $N \to \infty$. However, because of the shape of the velocity field induced by individual vortices, the convergence is extremely slow and power-law tails are still important for systems of $N \approx 10^6$ vortices.

Weiss et al (1998) have shown that the motion of individual vortices can be decomposed into three main regimes, namely: (*a*) slow motions induced by the mean velocity field generated by the other vortices. This motion is associated with the Gaussian, low-velocity part of the velocity PDF, and it generates a short-time exponential decay of the Lagrangian velocity autocorrelation. In this regime, the vortex motion can be approximated by a stochastic Ornstein-Uhlenbeck (OU) process (e.g. Wax 1954, van Dop et al 1985)

$$d\mathbf{x} = \mathrm{V}dt; \quad d\mathrm{V} = -\frac{\mathrm{V}}{T_{ou}}dt + \frac{\sigma_{ou}}{T_{ou}^{1/2}}d\mathrm{W}, \tag{21}$$

where $d\mathrm{W}$ is the Wiener process, a Gaussian random increment with $\langle d\mathrm{W}\rangle = 0$ and $\langle dW_\alpha(t)dW_\beta(t')\rangle = 2\delta_{\alpha,\beta}\delta(t-t')\,dt$, and Greek subscripts indicate vector components. The OU process is characterized by two parameters: a velocity scale σ_{ou}, which can be determined by the variance of the gaussian core of the velocity PDF, and the Lagrangian integral time T_{ou}, which can be determined by the short-time exponential behavior of the autocorrelation, $R(\tau) \approx \exp(-\tau/T_{ou})$. (*b*) Strong interactions between same-sign vortices, leading to temporary vortex couples that spin rapidly around each other without a significant mean motion; and (*c*) strong interactions between vortices of opposite sign, leading to temporary dipoles that travel rapidly across the domain.

The strong vortex-vortex interactions induce a long memory in the system of vortices; as a consequence, the velocity autocorrelation tends to zero very slowly after the short-time exponential decay. Vortex ensembles with different initial conditions may thus display long-lasting significant differences in the velocity PDF, suggesting that ergodicity is reached—if ever—only on very long time scales (see also Weiss & McWilliams 1991).

In general, passive particles undergo a Lagrangian motion analogous to that of the vortices. Particles close to a vortex remain there for long times, and have an overall motion similar to that of the vortex, plus a fast rotational component. Particles in the background mainly feel the mean velocity field generated by the vortices, and their motion can be modeled by an OU process for most of

the time. However, these passive particles sometimes come quite close to a vortex and can temporarily participate in the vortex motion. For example, passive particles can be significantly displaced from their previous position if the vortex is undergoing a period of fast dipolar motion.

Useful information on the Lagrangian dynamics is provided by the absolute dispersion of vortices and of passively advected tracers. The dispersion of an ensemble of particles undergoing an OU process can be easily calculated, and it provides an interesting comparison. Figure 9 shows the time-dependent dispersion coefficient $K(t) = A^2(t)/2t$ for two long integrations of a system of 100 vortices and 100 passive particles, compared with the prediction for a OU process. The dispersion of the vortices and of the passive particles turns out to be very similar to each other, but definitely larger—at long times—than that of an OU process describing the background vortex motion. Weiss et al (1998) have shown that this behavior is due to the close interactions between opposite-sign vortices. The pairing of same-sign vortices does not produce any recognizable sign on absolute dispersion, since a pair of same-sign vortices moves similarly to a single vortex with circulation equal to the sum of the circulations of the individual components. By contrast, the long flights of the vortex dipoles induce an anomalously large dispersion that can be clearly observed. Anomalous behavior can also be detected in relative dispersion, as discussed by Viecelli (1990, 1993) for vortices on the infinite plane.

The above results indicate that a possible stochastic model for Lagrangian motions in point-vortex systems is a background OU process, punctuated by occasional long flights generated by the temporary pairing of opposite-sign vortices. The quantitative study of this model has not yet been pursued, and would be an intriguing issue.

7. *Dust, Bubbles and Vortices*

The passive tracers considered in previous sections are point-like particles having vanishing inertia with respect to the advecting fluid. For these particles, Equation 5 is a good dynamical model. Complications arise when the advected particles have finite relative inertia and/or finite size, as in the case of dust grains, gas bubbles and the floats and balloons used as Lagrangian tracers in the ocean and the atmosphere. In this case, the dynamical behavior of the advected tracers (hereinafter called "impurities") is qualitatively different from that of fluid particles, and new effects can be present (e.g. Stommel 1949, Maxey & Riley 1983, Smith & Spiegel 1985, Maxey 1987, Crisanti et al 1992, Elghobashi & Truesdell 1992, Wang et al 1992, Vasiliev & Neishtadt 1994, Marcu et al 1995, Tanga et al 1996).

The equations of motion of a finite-size, finite-inertia particle may become extremely complicated, as they depend, for example, on the shape of the particle

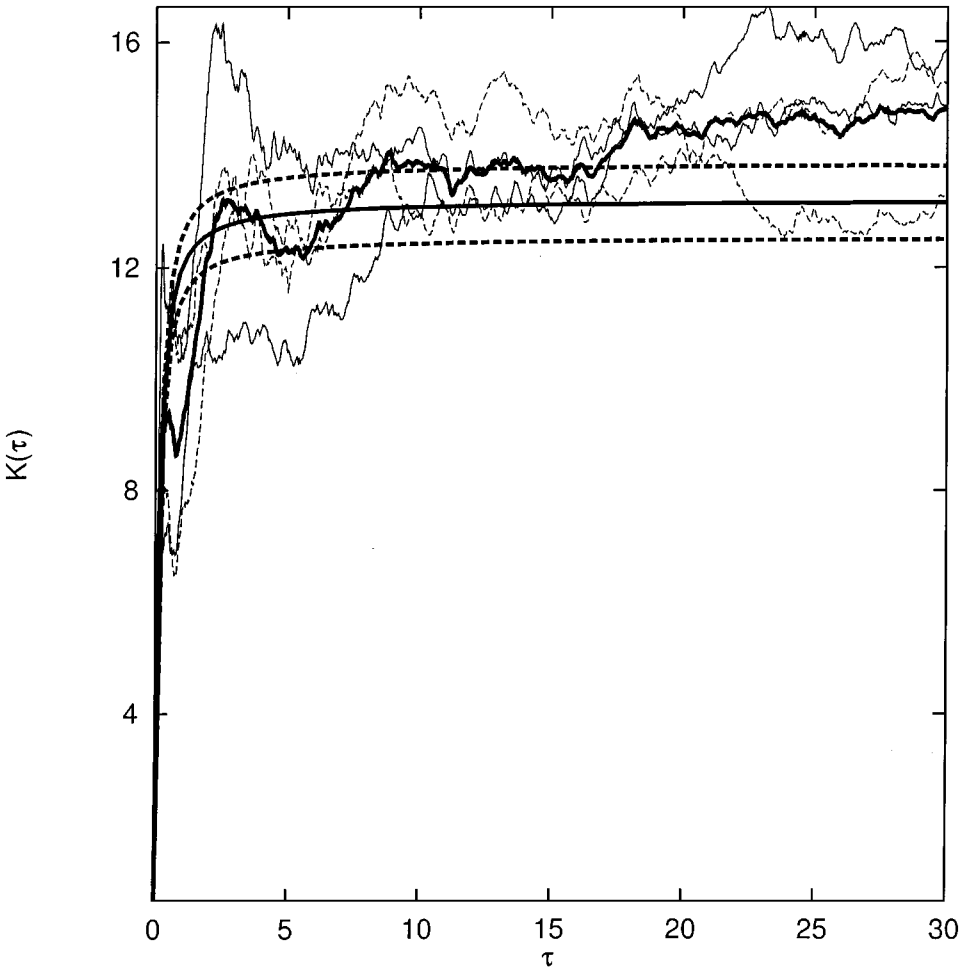

Figure 9 Absolute dispersion coefficient $K(t)$ from two long integrations of a system of 100 point vortices and 100 passive particles. *Thin solid curves* refer to vortex dispersion and *thin dashed curves* to passive particle dispersion. The *thick wiggly solid curve* is the average of the four dispersion coefficients. Also shown is the dispersion coefficient for an Ornstein-Uhlenbeck stochastic process (*thick, smooth solid curve*) and the envelope of expected error for four ensembles of 100 particles moving according to this process (*thick dashed curves*). Adapted from Weiss et al (1998).

itself (e.g. Auton et al 1988, Mallier & Maxey 1991). In the case of very small spherical particles, the equations of motion take a simple form that can be derived from Newton's second law of motion [see Maxey and Riley (1983) for a fairly complete discussion of the dynamical equations for small spherical impurities in nonrotating systems and Tanga et al (1996) for the rotating case].

In their simplest form, these equations take the form

$$\frac{d^2\mathbf{x}}{dt^2} = \delta\frac{D\mathbf{u}}{Dt} - \gamma\left(\frac{d\mathbf{x}}{dt} - \mathbf{u}\right) + \mathbf{g}(1 - \delta) - 2\Omega \times \left(\frac{d\mathbf{x}}{dt} - \delta\mathbf{u}\right) + |\Omega|^2 r(1-\delta)\hat{\mathbf{r}}, \tag{22}$$

where $\mathbf{x}$ is the position of the advected impurity, $\mathbf{u}$ is the Eulerian velocity field, r is the distance from the rotation axis, $\hat{\mathbf{r}}$ is the unit radial vector.

Let us now discuss the various terms of this equation. The term on the left hand side represents particle acceleration. The first term on the right hand side represents the force that the fluid would exert on a fluid particle placed at the position of the impurity, weighted by relative inertia. Here, $\delta = \rho_f/\rho_p$ is the ratio of the fluid density to the density of the individual impurity and the total time derivative $D\mathbf{u}/Dt = \partial\mathbf{u}/\partial t + \mathbf{u}\cdot\nabla\mathbf{u}$ is the material derivative following the fluid particle.

The second term on the right hand side represents the Stokes drag, and it models the friction that the fluid exerts on a particle moving with a velocity that is different from the local fluid velocity. The parameter γ may be written as $\gamma = (9\delta/2)(a/L)^{-2}Re^{-1}$, where a is the radius of the advected impurity, L is a typical scale of the Eulerian flow, and Re is the Reynolds number of the advecting flow.

The third term on the right hand side represents the buoyancy force acting on the impurity.

The fourth and fifth terms on the right hand side represent the relative Coriolis and centrifugal accelerations present in a rotating reference frame (such as the Earth or a rotating laboratory vessel); here Ω is the angular velocity of the system. In the absence of an advecting fluid ($\delta \to 0$), the Coriolis term takes the form $-2\Omega \times d\mathbf{x}/dt$ and the centrifugal term becomes $|\Omega|^2 r\hat{\mathbf{r}}$. When an advecting fluid is present, a term $-2\delta\Omega\times\mathbf{u}$ must be subtracted from the Coriolis term acting on the impurity because it has already been taken into account in the form of $\mathbf{u}$ and $D\mathbf{u}/Dt$. Thus, the Coriolis term present in Equation 22 acts on the density-weighted difference between the velocity of the impurity and that of the fluid. Analogously, the centrifugal term is proportional to $(1 - \delta)$ and it disappears for $\delta = 1$.

In writing Equation 22, we have discarded the added mass term, the Basset history term, and the so-called Faxen corrections (Maxey & Riley 1983). Previous work has indicated that these terms play a minor role for the type of flows we are concerned with here [see Maxey & Riley (1983), Tanga & Provenzale (1994); see also Thomas (1992) and Druzhinin & Ostrovsky (1994) for studies of the effect of the Basset term and Benjamin (1986) for a discussion of the added mass term].

The dynamics of Equation 22, have been studied by Crisanti et al (1992) for a kinematically prescribed two-dimensional incompressible flow defined by the stream function $\psi(x, y, t) = A \cos[x + B \sin(\sigma t)] \cos y$, in the absence of rotation ($\Omega = 0$). For a given functional form of the stream-function $\psi(x, y, t)$, the phase-space variables describing the motion of the advected impurities are $x, y, dx/dt, dy/dt$. These define a four-dimensional phase-space dynamics that can be autonomous or nonautonomous depending on the time dependence of the stream function. Note that Equation 22 is dissipative, and thus phase-space volumes shrink with time. This implies that the long-term evolution of the system takes place on a set of measure zero in the full phase space. This is a major difference with respect to the dynamics of fluid particles, described by an Hamiltonian system for which the Liouville theorem holds.

For a stationary stream funtion ($\sigma = 0$), Crisanti et al (1992) have shown that light particles tend to the elliptic fixed points at the center of the advection cells, while heavy particles undergo chaotic motion associated with the presence of a strange attractor in the four-dimensional phase space $(x, y, dx/dt, dy/dt)$. For time-dependent stream functions, the picture is more complicated and also light particles can display chaotic dynamics.

The motion of finite-inertia, finite-size impurities in barotropic turbulence has been studied by Provenzale et al (1998). Heavy particles in nonrotating turbulence are rapidly ejected from coherent vortices and strain-dominated cells, undergoing chaotic motion in the turbulent background where the Okubo-Weiss parameter is $Q \approx 0$. Thus, the coherent vortices become empty of heavy impurities. By contrast, light particles tend to enter the cores of coherent vortices and to be concentrated there, with possible filamentation events when the vortices are strained by strong vortex-vortex interactions.

The presence of an overall rotation of the system induces new effects in the dynamics of heavy impurities. When heavy particles are spinning inside a coherent vortex in a rotating reference frame, they are subject to two main opposing forces: the centrifugal force, which pushes the heavy particles outside the region of closed isolines, and the Coriolis force, which—for an overall cyclonic rotation of the reference frame—pushes the particles to the right of the direction of motion. Thus, the Coriolis force pushes heavy impurities out of cyclonic vortices and it pushes them toward the center of anticyclonic vortices.

While in a nonrotating reference frame heavy impurities are always ejected from coherent vortices, in rotation-dominated systems, the Coriolis force may become stronger than the centrifugal term when the Rossby number is small. As a consequence, heavy impurities can be concentrated in the cores of anticyclonic vortices (Tanga et al 1996, Provenzale et al 1998).

Figure 10 shows the evolved distribution of 8000 heavy impurities that were initially uniformly seeded in a statistically stationary numerical simulation of

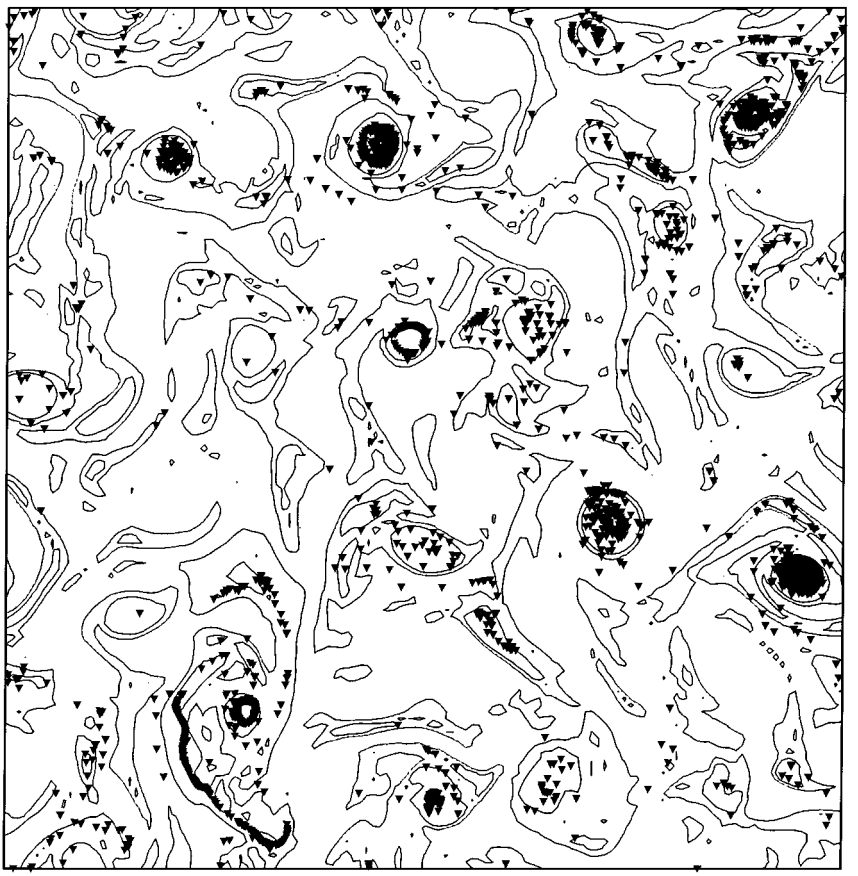

Figure 10 Distribution at $t = 6$ of 8000 heavy impurities advected by forced, statistically stationary two-dimensional turbulence in a cyclonically rotating reference frame. At $t = 0$, the impurities were seeded uniformly in the turbulent field. *Small solid triangles* indicate the positions of the advected impurities and *thin solid curves* indicate vorticity isolines. The impurities concentrate in the cores of anticyclonic vortices.

forced and dissipated 2D turbulence (Provenzale et al 1998). The same Eulerian velocity field discussed in Section 5 was used. The mean Eulerian integral time is $T_E = 0.14$ and the mean Lagrangian integral times $T_L = 0.035$. The overall rotation of the system is $\Omega = 160$ (in dimensionless units), which gives a rotation period $T_{rot} \approx 0.04$, of the same order of the Lagrangian integral time T_L. The impurities have $\delta = 0.8$ and $\gamma = 100$. The heavy particles concentrate inside the cores of the anticyclonic vortices, evacuating both the turbulent background and the cores of cyclonic vortices.

The concentration of heavy particles in anticyclonic vortices has been suggested by Barge & Sommeria (1995) and Tanga et al (1996) to play an important role in the formation of planetesimals in the early solar nebula. Present theories of Solar System formation favor building of the planets via progressive aggregation of dust grains in the primordial nebula (Taylor 1992). A crucial problem in this scenario is to reconcile the time scales for growth by accumulation of objects of the size of Jupiter and the estimated lifetime of the gaseous nebula itself. In particular, there is a lack of standard mechanisms for building planetesimals between the centimeter-sized grains formed by agglomeration and sticking and the larger objects capable of efficiently triggering gravitational instability.

By considering a simple kinematic flow field, Tanga et al (1996) have shown that if there are long-lived vortices on the early solar nebula, then a dust-concentrating mechanism such as that discussed above can push the dust grains into the cores of anticyclonic vortices, inducing a rapid formation of planetesimals which can then evolve by gravitational instability.

Clearly, this mechanism relies upon the existence of coherent vortices on the solar nebula. In a study of vortices on accretion disks, Bracco et al (1998) have shown that long-lived anticyclonic coherent vortices can effectively form in perturbed gaseous disks with cyclonic Keplerian rotation. Coherent vortices may thus play a crucial role in astrophysical disks, by radially transporting angular momentum and concentrating dust grains in their interior.

8. *Summary and Conclusions*

Coherent vortices play an important role in geophysical and astrophysical flows. In this review I have explored the transport properties of barotropic vortices, showing that vortices can trap fluid particles for long times and transport them during their motion.

Dispersion in vortex-dominated flows displays interesting signatures. Numerical simulation of 2D turbulence has indicated the existence of an anomalous absolute dispersion regime at intermediate times, associated with strain-dominated regions. Analysis of sub-surface float trajectories in the western North Atlantic has suggested the presence of a similar anomalous dispersion regime in ocean dynamics. The study of point-vortex systems has then suggested

that the motion of passively advected particles and of the vortices themselves can be described by a stochastic process where a background motion, obeying an Ornstein-Uhlenbeck process, is randomly punctuated by long flights of fast displacement, associated with the formation of temporary vortex dipoles.

Finally, coherent vortices in rotating reference frames can concentrate heavy particles in their cores. This has been suggested to be an important mechanism for the formation of planetesimals in the early solar nebula.

Even if some of the transport properties of coherent barotropic vortices are now reasonably understood, much work is still needed on this and other related subjects.

For example, baroclinic effects have been completely discarded in this review. The dynamics and merging properties of baroclinic vortices has been studied by several authors [see e.g. McWilliams & Flierl (1979), Hua & Haidvogel (1986), Griffiths & Hopfinger (1987), McWilliams (1989), Polvani et al (1989), Polvani (1991), Verron et al (1990), McWilliams et al (1994), Verron & Valcke (1994), Valcke & Verron (1997), Morel & McWilliams (1997), Sutyrin & Morel (1997)]. Preliminary work on the transport properties of baroclinic quasi-geostrophic vortices during merging events in numerical simulations with high vertical resolution (up to 256 layers) has shown that baroclinic vortices keep most of the trapping properties of their barotropic counterparts, possessing however a richer behavior that has to be carefully analyzed (von Hardenberg et al 1998).

In astrophysical flows, coherent vortices have been suggested to play an important role whenever the fluid is rapidly rotating. In most cases, magnetic effects cannot be discarded, and the vortices take the form of coherent magnetic flux tubes (Dowling & Spiegel 1990, Kinney et al 1995, Bracco et al 1998). A full study of coherent magnetic vortices and of their transport properties is still needed.

In geophysical flows, coherent vortices represent only one of the components of the rich spatiotemporal texture of geostrophic turbulence. Coherent jets and waves represent other components, and a full understanding of transport in geophysical turbulence requires the study of the behavior of each of these entities, as well as of their interplay. Similarly, the interaction of coherent vortices and jets with topography is another important topic.

Once the effects of coherent structures are understood, the time of parameterization will come. Until now, transport of passive tracers in large-scale ocean and atmosphere general circulation models has been parameterized by using various versions of eddy diffusion, or more refined parameterizations such as that proposed by Gent and McWilliams (1990). The results discussed in this review indicate that the simplest parameterizations cannot properly represent the complexity induced by a field of coherent eddies. Thus, new stochastic

processes must be developed, and their continuous limit understood, in order to obtain satisfactory eddy-transport operators to be included in large-scale general circulation models. But this is still matter for future research.

ACKNOWLEDGMENTS

Most of the material discussed here is the product of collaborations with several colleagues and friends all over the world. In particular, I am grateful to Armando Babiano, who triggered my interest in turbulence by his deep knowledge of turbulent behavior; to James C McWilliams and Jeffrey B Weiss for many interesting discussions an comments about science and life; to B Lien Hua, who pushed me to become a little wetter by looking at subsurface float trajectories; and to Edward A Spiegel for his attempts to broaden my view and for disrespectful comments. Many thanks to Annalisa Bracco, who has corrected most of the mistakes in our numerical codes, and to Jost Hardenberg, who has run the (corrected) codes on whatever computer he was able to find. I am also grateful to Elena Carena, Luca Montabone, Giuseppe Murante, Claudia Pasquero, and Francesco Paparella, who helped me, one way or another, during the writing of these notes.

Literature Cited

Abramowicz MA, Lanza A, Spiegel EA, Szuszkiewicz E. 1991. Vortices on accretion disks. *Nature* 356:41–43

Adem J. 1956. A series solution for the barotropic vorticity equation and its application in the study of atmospheric vortices. *Tellus* 8:364–72

Aref H. 1983. Integrable, chaotic, and turbulent vortex motion in two-dimensional flows. *Annu. Rev. Fluid Mech.* 15:345–89

Aref H, Jones SW, Mofina S, Zawadzki I. 1989. Vortices, kinematics and chaos. *Physica D* 37:423–40

Aref H, Pomphrey N. 1980. Integrable and chaotic motions of four vortices. *Phys. Lett. A* 78:297–300

Armi L, Herbert D, Oakey N, Price JF, Richardon PL, et al. 1989. Two years in the life of a Mediterranean salt lens. *J. Phys. Oceangr.* 19:354–70

Artale A, Boffetta G, Celani A, Cencini M, Vulpiani A. 1997. Dispersion of passive tracers in closed basins: beyond the diffusion coefficient. *Phys. Fluids* 9:3162–71

Auton TR, Hunt JCR, Prud'homme M. 1988. The force exerted on a body in inviscid unsteady non-uniform rotational flow. *J. Fluid Mech.* 197:241–57

Babiano A, Basdevant C, Legras B, Sadourny R. 1987a. Vorticity and passive-scalar dynamics in two-dimensional turbulence. *J. Fluid Mech.* 183:379–97

Babiano A, Basdevant C, LeRoy P, Sadourny R. 1987b. Single-particle dispersion, Lagrangian structure function and Lagrangian energy spectrum in two-dimensional incompressible turbulence. *J. Mar. Res.* 45:107–31

Babiano A, Basdevant C, LeRoy P, Sadourny R. 1990. Relative dispersion in two-dimensional turbulence. *J. Fluid Mech.* 214:535–57

Babiano A, Boffetta G, Provenzale A, Vulpiani A. 1994. Chaotic advection in point vortex models and two-dimensional turbulence. *Phys. Fluids* 6:2465–74

Babiano A, Dubrulle B, Frick P. 1995. Scaling properties of two-dimensional turbulence. *Phys. Rev. E* 52:3719–29

Barge P, Sommeria J. 1995. Did planet formation begin inside persistent gaseous vortices? *Astron. Astrophys.* 295:L1–L4

Bartello P, Holloway G. 1991. Passive scalar transport in β-plane turbulence. *J. Fluid Mech.* 223:521–36

Bartello P, Warn T. 1996. Self-similarity of decaying two-dimensional turbulence. *J. Fluid Mech.* 326:357–72

Basdevant C, Legras B, Sadourny R, Beland M. 1981. A study of barotropic model flow: intermittency waves and predictability. *J. Atmos. Sci.* 38:2305–26

Basdevant C, Philipovitch T. 1994. On the validity of the "Weiss criterion" in two-dimensional turbulence. *Physica D* 73:17–30

Batchelor GK. 1969. Computation of the energy spectrum in homogeneous two-dimensional turbulence. *Phys. Fluids Suppl.* 12:II-233–39

Benettin G, Galgani L, Strelcyn JM. 1976. Kolmogorov entropy and numerical experiments. *Phys. Rev. A* 14:2338–45

Benettin G, Giorgilli A, Galgani L, Strelcyn JM. 1980. Lyapunov characteristic exponents for smooth dynamical systems and for Hamiltonian systems; a method for computing all of them. Part 1: Theory. Part 2: Numerical applications. *Meccanica* 15:9–21

Bengston L, Lighthill J, eds. 1982. *Intense Atmospheric Vortices.* Berlin: Springer-Verlag

Benjamin TB. 1986. Note on added mass and drift. *J. Fluid Mech.* 169:251–56

Benzi R, Colella M, Briscolini M, Santangelo P. 1992. A simple point vortex model for two-dimensional decaying turbulence. *Phys. Fluids A* 4:1036–39

Benzi R, Paladin G, Patarnello S, Santangelo P, Vulpiani A. 1986. Intermittency and coherent structures in two-dimensional turbulence. *J. Phys. A: Math. Gen.* 19:3771–84

Benzi R, Patarnello S, Santangelo P. 1987. On the statistical properties of two-dimensional decaying turbulence. *Europhys. Lett.* 3:811–18

Boffetta G, Celani A, Franzese P. 1996. Trapping of passive tracers in a point vortex system. *J. Phys. A: Math. Gen.* 29:3749–59

Borue V. 1994. Inverse energy cascade in stationary two-dimensional homogeneous turbulence. *Phys. Rev. Lett.* 72:1475–78

Bracco A, Provenzale A, Spiegel EA, Yecko P. 1998. Spotted disks. In *Theory of Black Hole Accretion Disks*, ed. M Abramowicz, G Bjornson, J Pringle. Cambridge, UK: Cambridge Univ. Press. In press

Brachet M, Meneguzzi M, Politano H, Sulem P. 1988. The dynamics of freely decaying two-dimensional turbulence. *J. Fluid Mech.* 194:333–49

Brummell NH, Hurlburt NE, Toomre J. 1996. Turbulent compressible convection with rotation. I. Flow structure and evolution. *Astrophys. J.* 473:494–513

Canuto C, Hussaini MY, Quarteroni A, Zang TA. 1987. *Spectral Methods in Fluid Dynamics*. Berlin: Springer-Verlag. 567 pp.

Carena E, Provenzale A, Weiss JB. 1998. Eulerian and Lagrangian statistics in point-vortex systems. *Ann. Geophys.* 16:C1110

Carnevale GF, Kloosterziel RC. 1994. Lobe shedding from propagating vortices. *Physica D* 76:147–67

Carnevale GF, McWilliams JC, Pomeau Y, Weiss JB, Young WR. 1991. Evolution of vortex statistics in two-dimensional turbulence. *Phys. Rev. Lett.* 66:2735–37

Chan JCL, Williams RT. 1987. Analytical and numerical studies of the beta-effect in tropical cyclone motion. Part I: Zero mean flow. *J. Atmos. Sci.* 44:1257–65

Charney J. 1971. Geostrophic turbulence. *J. Atmos. Sci.* 28:1087–95

Chavanis P-H, Sommeria J. 1996. Classification of self-organized vortices in two-dimensional turbulence: the case of a bounded domain. *J. Fluid Mech.* 314:267–97

Couder Y. 1984. Two dimensional grid turbulence in a thin liquid film. *J. Phys. Lett.* 45: 353–60

Couder Y, Basdevant C. 1986. Experimental and numerical study of vortex couples in two-dimensional flows. *J. Fluid Mech.* 173:225–51

Crisanti A, Falcioni M, Paladin G, Vulpiani A. 1991. Lagrangian chaos: transport, mixing and diffusion in fluids. *Riv. Nuovo Cimento* 14(12):1–80

Crisanti A, Falcioni M, Provenzale A, Tanga P, Vulpiani A. 1992. Dynamics of passively advected impurities in simple two-dimensional flow models. *Phys. Fluids A* 4:1805–20

Danabasoglu G, McWilliams JC, Gent PR. 1994. The role of mesoscale tracer transports in the global ocean circulation. *Science* 264:1123–26

Dewar WK, Flierl GR. 1985. Particle trajectories and simple models of transport in coherent vortices. *Dyn. Atmos. Oceans* 9:215–52

Dowling TE. 1995. Dynamics of Jovian atmospheres. *Annu. Rev. Fluid Mech.* 27:293–334

Dowling TE, Spiegel EA. 1990. Stellar and Jovian vortices. *Ann. NY Acad. Sci.* 617:190–216

Dritschel DG. 1993. Vortex properties of two-dimensional turbulence. *Phys. Fluids A* 5: 984–97

Dritschel DG. 1995. A general theory for two-dimensional vortex interactions. *J. Fluid Mech.* 293:269–303

Dritschel DG, Waugh DW. 1992. Quantification of the inelastic interaction of unequal vortices in two-dimensional vortex dynamics. *Phys. Fluids A* 4:1737–44

Dritschel DG, Zabusky NJ. 1996. On the nature of vortex interactions and models in unforced

nearly-inviscid two-dimensional turbulence. *Phys. Fluids* 8:1256–61
Druzhinin OA, Ostrovsky LA. 1994. The influence of Basset force on particle dynamics in two-dimensional flows. *Physica D* 76:34–43
Eckmann J-P, Ruelle D. 1985. Ergodic theory of chaos and strange attractors. *Rev. Mod. Phys.* 57:617–56
Elghobashi S, Truesdell GC. 1992. Direct simulation of particle dispersion in decaying isotropic turbulence. *J. Fluid Mech.* 242:655–700
Elhmaidi D, Provenzale A, Babiano A. 1993. Elementary topology of two-dimensional turbulence from a Lagrangian viewpoint and single-particle dispersion. *J. Fluid Mech.* 257:533–58
Firing E, Beardsley RC. 1976. The behavior of a barotropic eddy on a β-plane. *J. Phys. Oceangr.* 6:57–65
Flierl GR. 1987. Isolated eddy models in geophysics. *Annu. Rev. Fluid Mech.* 19:493–530
Flierl GR, Stern ME, Whitehead JA Jr. 1983. The physical significance of modons: Laboratory experiments and general integral constraints. *Dyn. Atmos. Oceans* 7:223–63
Fornberg B. 1978. A numerical study of 2D turbulence. *J. Comput. Phys.* 25:1–31
Frisch U, Sulem PL. 1984. Numerical simulation of the inverse cascade in two-dimensional turbulence. *Phys. Fluids* 27:1921–23
Gent PR, McWilliams JC. 1990. Isopycnal mixing in ocean circulation models. *J. Phys. Oceangr.* 20:150–55
Griffiths RW, Hopfinger EJ. 1987. Coalescing of geostrophic vortices. *J. Fluid Mech.* 178:73–97
Hasegawa A, Mima K. 1978. Pseudo-3-dimensional turbulence in magnetized nonuniform plasma. *Phys. Fluids* 21:87–92
Herring JR, McWilliam JC. 1984. Comparison of direct numerical simulation of two-dimensional turbulence with two-point closure: the effects of intermittency. *J. Fluid Mech.* 153:229–42
Hopfinger EJ, van Heijst GJF. 1993. Vortices in rotating fluids. *Annu. Rev. Fluid Mech.* 25: 241–89
Hua BL, Haidvogel DB. 1986. Numerical simulations of the vertical structure of quasi-geostrophic turbulence. *J. Atmos. Sci.* 43: 2923–36
Hua BL, Klein P. 1998. An exact criterion for the stirring properties of nearly two-dimensional turbulence. *Physica D.* In press
Ingersoll AP. 1990. Atmospheric dynamics of the outer planets. *Science* 248:308–15
Julien K, Legg S, McWilliams J, Werne J. 1996. Rapidly rotating turbulent Rayleigh-Benard convection. *J. Fluid Mech.* 322:243–73
Killworth PD. 1983. Deep convection in the world oceans. *Rev. Geophys.* 21:1–26
Kinney R, McWilliams JC, Tajima C. 1995. Coherent structures and turbulent cascades in two-dimensional incompressible magnetohydrodynamic turbulence. *Phys. Plasmas* 2:3623–39
Kirchhoff GR. 1876. *Vorlesungen uber Matematische Physik*, Vol. 1. Leipzig: Teubner. 466 pp.
Korotaev GK, Fedotov AB. 1994. Dynamics of an isolated barotropic vortex on a beta-plane. *J. Fluid Mech.* 264:277–301
Kraichnan RH. 1967. Inertial ranges in two-dimensional turbulence. *Phys. Fluids* 10:1417–23
Kraichnan RH, Montgomery D. 1980. Two-dimensional turbulence. *Rep. Prog. Phys.* 43:547–619
Kukharkin N, Orszag SA, Yakhot V. 1995. Quasicrystallization of vortices in driftwave turbulence. *Phys. Rev. Lett.* 75:2486–89
Kuznetsov L, Zaslavsky GM. 1998. Chaotic dynamics of passive particles in three-vortex systems. I. Dynamical analysis. In *Chaos, Kinetics, and Nonlinear Dynamics in Fluids and Plasmas*, ed. S Benkadda, GM Zaslavsky, pp. 119–31. Berlin: Springer-Verlag
Larcheveque M. 1990. Pressure fluctuations and lagrangian accelerations in two-dimensional incompressible isotropic turbulence. *Eur. J. Mech. B* 9:109–28
Larichev VD, McWilliams JC. 1991. Weakly decaying turbulence in an equivalent-barotropic fluid. *Phys. Fluids* A 3:938–50
Legras B, Santangelo P, Benzi R. 1988. High-resolution numerical experiments for forced two-dimensional turbulence. *Europhys. Lett.* 5:37–42
Leith CE. 1968. Diffusion approximation for two-dimensional turbulence. *Phys. Fluids* 11: 671–73
Leith CE. 1984. Minimum enstrophy vortices. *Phys. Fluids* 27:1388–95
Lesieur M. 1987. *Turbulence in Fluids*. Dordrecht: Kluwer. 281 pp.
Lilly DK. 1972. Numerical simulation studies of two-dimensional turbulence: Part 1. Models of statistically steady turbulence. *Geophys. Fluid Dyn.* 3:290–319
Llewellyn-Smith SG. 1996. The motion of a nonisolated vortex on the β-plane. *J. Fluid Mech.* 346:149–79
Malanotte Rizzoli P. 1982. Planetary waves in geophysical flows. *Adv. Geophys.* 24:147
Mallier R, Maxey M. 1991. The settling of nonspherical particles in a cellular flow field. *Phys. Fluids* A 3:1481–94
Maltrud EM, Vallis GK. 1991. Energy spectra and coherent structures in forced two-

dimensional and beta-plane turbulence. *J. Fluid Mech.* 228:321–42
Maltrud EM, Vallis GK. 1993. Energy and enstrophy transfer in numerical simulations of two-dimensional turbulence. *Phys. Fluids A* 5:1760–75
Marcu B, Meiburg E, Newton PK. 1995. Dynamics of heavy particles in a Burgers vortex. *Phys. Fluids* 7:400–10
Matthaeus WH, Stribling WT, Martinez D, Oughton S, Montgomery D. 1991. Decaying two-dimensional Navier-Stokes turbulence at very long times. *Physica D* 51:531
Maxey MR. 1987. The motion of small spherical particles in a cellular flow field. *Phys. Fluids* 30:1915–28
Maxey MR, Riley JJ. 1983. Equation of motion for a small rigid sphere in a nonuniform flow. *Phys. Fluids* 26:883–89
McIntyre ME. 1989. On the Antarctic ozone hole. *J. Atmos. Terr. Phys.* 51:29–43
McIntyre ME. 1995. The stratospheric polar vortex and sub-vortex: fluid dynamics and midlatitude ozone loss. *Philos. Trans. R. Soc. London Ser. A* 352:227–40
McWilliams JC. 1984. The emergence of isolated coherent vortices in turbulent flow. *J. Fluid Mech.* 146:21–43
McWilliams JC. 1985. Submesoscale, coherent vortices in the ocean. *Rev. Geophys.* 23:165–82
McWilliams JC. 1989. Statistical properties of decaying geostrophic turbulence. *J. Fluid Mech.* 198:199–230
McWilliams JC. 1990a. The vortices of two-dimensional turbulence. *J. Fluid Mech.* 219: 361–85
McWilliams JC. 1990b. A demonstration of the suppression of turbulent cascades by coherent vortices in two-dimensional turbulence. *Phys. Fluids A* 2:547–52
McWilliams JC. 1996. Modeling the oceanic general circulation. *Annu. Rev. Fluid Mech.* 28:215–48
McWilliams J, Flierl GR. 1979. On the evolution of isolated, nonlinear vortices. *J. Phys. Oceangr.* 9:1155–82
McWilliams JC, Weiss JB. 1994. Anisotropic geophysical vortices. *CHAOS* 4:305–11
McWilliams JC, Weiss JB, Yavneh I. 1994. Anisotropy and coherent vortex structures in planetary turbulence. *Science* 264:410–13
Meleshko VV, Konstantinov MY, Gurzhi AA, Konovaljuk TP. 1992. Advection of a vortex pair atmosphere in a velocity field of point vortices. *Phys. Fluids A* 4:2779–97
Min IA, Mezic I, Leonard A. 1996. Levy stable distributions for velocity and velocity difference in systems of vortex elements. *Phys. Fluids* 8:1169–80
MODE Group. 1978. The Mid-Ocean Dynamics Experiment. *Deep-Sea Res.* 25:859–910
Monin AS, Yaglom AM. 1971. *Statistical Fluid Mechanics*. Cambridge, MA: MIT Press. 769 pp.
Morel Y, McWilliams JC. 1997. Evolution of isolated interior vortices in the ocean. *J. Phys. Oceangr.* 27:727–48
Nezlin MV, Snezhkin EN. 1993. *Rossby vortices, spiral structures, solitons*. Berlin: Springer-Verlag. 223 pp.
Ohkitani K. 1991. Wavenuber space dynamics of enstrophy cascade in a forced two-dimensional turbulence. *Phys. Fluids A* 3:1598–1611
Okubo A. 1970. Horizontal dispersion of floatable particles in the vicinity of velocity singularities such as convergences. *Deep-Sea Res.* 17:445–54
Orszag S. 1971. Numerical simulation of incompressible flows within simple boundaries: 1. Galerkin (spectral) representations. *Stud. Appl. Math.* L:293–328
Ottino JM. 1989. *The Kinematics of Mixing: Stretching, Chaos, and Transport*. Cambridge, UK: Cambridge Univ. Press. 364 pp.
Ottino JM. 1990. Mixing, chaotic advection, and turbulence. *Annu. Rev. Fluid Mech.* 22: 207–53
Owens WB. 1991. A statistical description of the mean criculation and eddy variability in the western North Atlantic using SOFAR floats. *Progr. Oceanogr.* 28:257–303
Paparella F, Babiano A, Basdevant C, Provenzale A, Tanga P. 1997. A Lagrangian study of the Antarctic polar vortex. *J. Geophys. Res.* 102:6765–73
Pedlosky J. 1987. *Geophysical Fluid Dynamics*. New York: Springer-Verleg. 710 pp.
Pentek A, Tel T, Toroczkai Z. 1995. Chaotic advection in the velocity field of leapfrogging vortex pairs. *J. Phys. A: Math. Gen.* 28:2191–216
Pierrehumbert RT. 1991a. Large-scale horizontal mixing in planetary atmospheres. *Phys. Fluids A* 2:1250–60
Pierrehumbert RT. 1991b. Chaotic mixing of tracer and vorticity by modulated travelling Rossby waves. *Geophys. Astrophys. Fluid Dyn.* 58:285–319
Pierrehumbert RT, Yang H. 1993. Global chaotic mixing on isentropic surfaces. *J. Atmos. Sci.* 50:2462–80
Polvani LM. 1991. Two-layer geostrophic vortex dynamics. Part 2. Alignment and two-layer V-states. *J. Fluid Mech.* 225:241–70
Polvani LM, Zabusky NJ, Flierl GR. 1989. Two-layer geostrophic vortex dynamics. Part 1. Upper V-states and merger. *J. Fluid Mech.* 105:215–42
Provenzale A, Babiano A, Villone B. 1995.

Single-particle trajectories in two-dimensional turbulence. *Chaos. Solit. Fract.* 5: 2055–71

Provenzale A, Babiano A, Zanella A. 1998. Dynamics of Lagrangian tracers in barotropic turbulence. In *Mixing: Chaos and Turbulence*, ed. H Chate, JM Chomaz, E Villermaux. New York: Plenum. In press

Reznik GM, Dewar WK. 1994. An analytical theory of distributed axisymmetric vortices on the β-plane. *J. Fluid Mech.* 269:301–21

Rhines PB. 1975. Waves and turbulence on a beta-plane. *J. Fluid Mech.* 69:417–43

Rhines PB. 1979. Geostrophic turbulence. *Annu. Rev. Fluid Mech.* 11:401–41

Rhines PB, Young WR. 1983. How rapidly is a passive scalar mixed within closed streamlines? *J. Fluid Mech.* 133:133–45

Riccardi G, Piva R, Benzi R. 1995. A physical model for merging in two-dimensional decaying turbulence. *Phys. Fluids* 7:3091–104

Richardson PL, McCartney MS, Maillard C. 1991. A search for meddies in historical data. *Dyn. Atmos. Oceans* 15:241–65

Richardson PL, Price J, Owens WB, Schmitz WJ, Rossby HT, et al. 1981. North Atlantic subtropical gyre: SOFAR floats tracked by moored listening stations. *Science* 213:435–37

Richardson PL, Walsh D, Armi L, Schroder M, Price JF. 1989. Tracking three meddies with SOFAR floats. *J. Phys. Oceangr.* 19:371–83

Ring Group. 1981. Gulf Stream cold core rings: their physics, chemistry and biology. *Science* 212:1091–1100

Robert R, Sommeria J. 1991. Statistical equilibrium states for two-dimensional turbulence. *J. Fluid Mech.* 229:291–310

Rom-Kedar V, Leonard A, Wiggins S. 1990. An analytical study of transport, mixing and chaos in an unsteady vortical flow. *J. Fluid Mech.* 214:347–58

Rossby CG. 1949. On a mechanism for the release of potential energy in the atmosphere. *J. Met.* 6:163–80

Rupolo V, Hua BL, Provenzale A, Artale V. 1996. Lagrangian velocity spectra at 700 m in the western North Atlantic. *J. Phys. Oceangr.* 26:1591–607

Santangelo P, Benzi R, Legras B. 1989. The generation of vortices in high-resolution, two-dimensional decaying turbulence and the influence of initial conditions on the breaking of self-similarity. *Phys. Fluids A* 1:1027–34

Smith LA, Spiegel EA. 1985. Pattern formation by particles settling in viscous flows. In *Macroscopic Modelling of Turbulent Flows*, ed. U Frisch, JB Keller, G Papanicolaou, O Pironneau, pp. 306–18. Berlin: Springer-Verlag

Solomon TH, Weeks ER, Swinney HL. 1993. Observation of anomalous diffusion and Levy flights in a two-dimensional rotating flow. *Phys. Rev. Lett.* 71:3975–78

Solomon TH, Weeks ER, Swinney HL. 1994. Chaotic advection in a two-dimensional flow: Levy flights and anomalous diffusion. *Physica D* 76:70–84

Stommel H. 1949. Trajectories of small bodies sinking slowly through convection cells. *J. Mar. Res.* 8:24–29

Sutyrin GG, Flierl GR. 1994. Intense vortex motion on the beta plane: development of the beta gyres. *J. Fluid Mech.* 268:103–31

Sutyrin GG, Hesthaven JS, Lynov JS, Rasmussen JJ. 1994. Dynamical properties of vortical structures on the beta-plane. *J. Fluid Mech.* 268:103–31

Sutyrin GG, Morel Y. 1997. Intense vortex motion in a sratified fluid on the beta-plane: an analytical theory and its validation. *J. Fluid Mech.* 336:203–20

Tanga P, Babiano A, Dubrulle B, Provenzale A. 1996. Forming planetesimals in vortices. *ICARUS* 121:158–70

Tanga P, Provenzale A. 1994. Dynamics of advected tracers with varying buoyancy. *Physica D* 76:202–15

Taylor GI. 1921. Diffusion by continuous movement. *Proc. London. Math. Soc.* 20:196–212

Taylor SR. 1992. *Solar System Evolution: A New Perspective*. Cambridge, UK: Cambridge Univ. Press. 307 pp.

Thomas PJ. 1992. On the influence of the Basset history force on the motion of a particle through a fluid. *Phys. Fluids A* 4:2090–93

Valcke S, Verron J. 1997. Interactions of baroclinic isolated vortices: the dominant effect of shielding. *J. Phys. Oceangr.* 27:525–41

van Dop H, Nieuwstadt FTM, Hunt JCR. 1985. Random walk models for particle displacements in inhomogeneous unsteady turbulent flows. *Phys. Fluids* 28:1636–53

Vasiliev AA, Neishtadt AI. 1994. Regular and chaotic transport of impurities in steady flows. *CHAOS* 4:673–80

Velasco Fuentes OU. 1994. Propagation and transport properties of dipolar vortices on a γ plane. *Phys. Fluids* 6:3341–52

Velasco Fuentes OU, van Heijst GJF, Cremers BE. 1995. Chaotic transport by dipolar vortices on a β-plane. *J. Fluid Mech.* 291:139–61

Verron J, Hopfinger EJ, McWilliams JC. 1990. Sensitivity to initial conditions in the merging of two-layer baroclinic vortices. *Phys. Fluids A* 2:886–89

Verron J, Valcke S. 1994. Scale-dependent merging of baroclinic vortices. *J. Fluid Mech.* 264:81–106

Viecelli JA. 1990. Dynamics of two-dimensional turbulence. *Phys. Fluids A* 2:2036–45

Viecelli JA. 1993. Statistical mechanics and

correlation properties of a rotating two-dimensional flow of like-sign vortices. *Phys. Fluids A* 5:2484–501

von Hardenberg JD, Provenzale A, McWilliams JC, Shchepetkin AS, Weiss JB. 1998. Vortex merging in quasigeostrophic flows: a Lagrangian view. *Ann. Geophys.* 16:C1156

Wang LP, Maxey MR, Burton TD, Stock DE. 1992. Chaotic dynamics of particle dispersion in fluids. *Phys. Fluids A* 4:1789–804

Waugh DW. 1992. The efficiency of symmetric vortex merger. *Phys. Fluids A* 4:1745–58

Wax N, ed. 1954. *Selected Papers on Noise and Stochastic Processes.* New York: Dover. 337 pp.

Weiss J. 1991. The dynamics of enstrophy transfer in two-dimensional hydrodynamics. *Physica D* 48:273–94

Weiss JB, McWilliams JC. 1991. Nonergodicity of point vortices. *Phys. Fluids A* 3:835–44

Weiss JB, McWilliams JC. 1993. Temporal scaling behavior of decaying two-dimensional turbulence. *Phys. Fluids A* 5:608–21

Weiss JB, Provenzale A, McWilliams JC. 1998. Lagrangian dynamics in high-dimensional point-vortex systems. *Phys. Fluids.* In press

Wiggins S. 1992. *Chaotic Transport in Dynamical Systems.* New York: Springer

Wunsch C. 1981. Low frequency variability in the sea. In *Evolution of Physical Oceanography*, ed. BA Warren, C Wunsch, pp. 342–75. Cambridge, MA: MIT Press

Annual Review of Fluid Mechanics
Volume 31, 1999

CONTENTS